CHALMERS
UNIVERSITY OF TECHNOLOGY

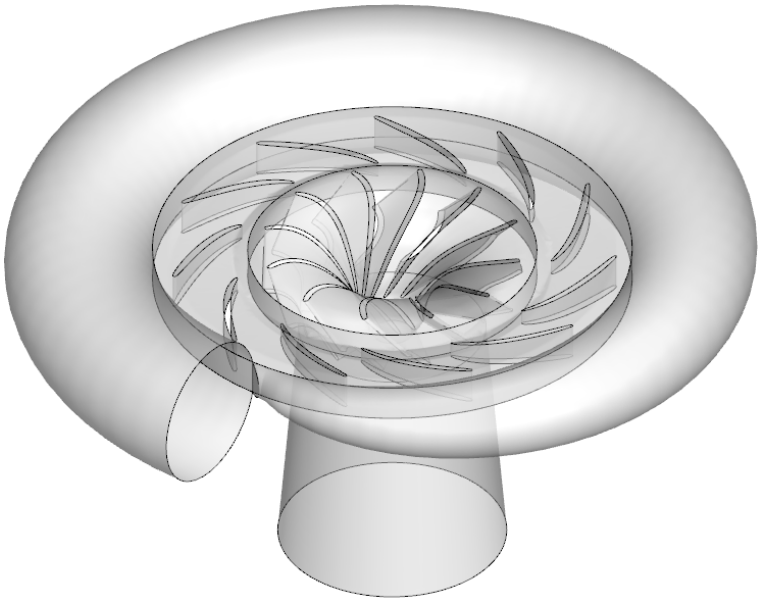

Conceptual design tool for radial turbines

Master's Thesis in Applied Mechanics

Elias Mikael Vagn Siggeirsson
Steinn Gunnarsson

Department of Applied Mechanics
Chalmers University of Technology
Gothenburg, Sweden 2015-08-05
Master's Thesis 2015:67

Master's thesis 2015:67

Conceptual design tool for radial turbines

Verification of the coherence between a generic fluid radial turbine mean line design code and macro based CFD simulations

Elias Mikael Vagn Siggeirsson
Steinn Gunnarsson

Department of Applied Mechanics
Division of Fluid Dynamics
Chalmers University of Technology
Gothenburg, Sweden 2015

Conceptual design tool for radial turbines
Verification of the coherence between a generic fluid radial turbine mean line design code and macro based CFD simulations
Elias Mikael Vagn Siggeirsson
Steinn Gunnarsson

Supervisor: Oskar Thulin, Applied Mechanics
Examiner: Thomas Grönstedt, Applied Mechanics

Master's Thesis 2015:67
Department of Applied Mechanics
Division of Fluid Dynamics
Chalmers University of Technology
SE-412 96 Gothenburg
Telephone +46 31 772 1000

Cover: Nasa test case model of a radial turbine.

Typeset in LaTeX
Printed by Chalmers University of Technology Reproservice
Gothenburg, Sweden 2015

Conceptual design tool for radial turbines
Verification of the coherence between a generic fluid radial turbine mean line design code and macro based CFD simulations

Elias Mikael Vagn Siggeirsson
Steinn Gunnarsson
Department of Applied Mechanics
Chalmers University of Technology

Abstract

The aim of this thesis is to develop a method to automate the set up process of a CFD simulation and study the flow of a generic fluid radial turbine design. This method could then be used to verify the coherence between an in-house mean line design performance code and 3D CFD simulations in a robust and simple way. The method can be used as a conceptual design tool for radial turbines and supports most fluids included in the REFPROP™ software database. To show the capability of the method developed, without going into full analysis with mesh dependent study and as high quality mesh as possible, a comparison is made between the performance code and the 3D CFD simulations. The turbine analysis is carried out using the methods of Computational Fluid Dynamics (CFD) and Finite Element Analysis (FEA) for structural analysis. Two methods have been developed for the simulations: one rapid Single Blade Passage (SBP) model as well as a more detailed Full Turbine (FT) model. The macro based methodology described in the report has proven to reduce the set up time for the simulation of the radial turbine extracted from the performance code. Two cases are used for comparison between the performance code and the 3D CFD simulations. The first one is based on an experimental report from NASA, a cold performance evaluation of a 6.02 inch radial inflow turbine with Argon fluid. The efficiency given in the report is similar to the result from the performance code and the CFD simulation. The other case is an Organic Rankine Cycle (ORC) turbine with refrigerant R143a as a working fluid. The efficiency in the CFD simulations is slightly lower than the performance code possibly due to partly choked flow. Both test cases show similar behaviour with respect to flow separation and highlight possible improvements in the performance code. A number of programs from ANSYS™ are used to carry out the thesis work. The programs are DesignModeler™ and ICEM CFD™ for CAD modeling, TurboGrid™ and ICEM CFD™ for meshing, CFX™ is used as the CFD solver and Mechanical™ for structural analysis.

Acknowledgements

We would like to thank our supervisor, Oskar Thulin (Division of Fluid Mechanics), and our examiner, Tomas Grönstedt (Division of Fluid Mechanics), for guidance and support throughout this work and for always being open to discussions. We would also like to thank Olivier Petit (Division of Fluid Mechanics) for valuable advice and help with the CFD part.

Elias Mikael Vagn Siggeirsson and Steinn Gunnarsson, Göteborg September 24, 2015

Contents

Nomenclature

Abbreviations

APU Auxiliary Power Unit

ATM Automatic Topology and Meshing

CAD Computer Aided Design

CCL CFX Command Language

CEL CFX Expression Language

CFD Computational Fluid Dynamics

FEA Finite Element Analysis

FSI Fluid Structural Interaction

FT Full Turbine

FVM Finite Volume Method

LE Leading Edge

NURBS Non-Uniform Rational Basis Spline

ORC Organic Rankine Cycle

RANS Reynolds Averaged Navier Stokes

RSM Reynolds Stress Model

SBP Single Blade Passage

SBPTC Single Blade Passage with Tip Clearance

SST Shear Stress Transport

TE Trailing Edge

$URANS$ Unsteady Reynolds Averaged Navier Stokes

Greek Symbols

δ_{ij} Identity matrix

η Efficiency

λ Thermal conductivity

μ Dynamic viscosity

ν Kinematic viscosity

Ω Angular velocity

ω Turbulence frequency

Ω_s Specific speed

Π Pressure ratio

ρ Density

σ Normal stress

σ_y Yield stress

τ Shear stress

τ_A Axial torque

θ Diffuser angle

ε Dissipation

Roman Symbols

$\dot{W}_x$ Shaft work

A Cross sectional area

B Blockage

C Velocity

c Velocity

C_f Skin friction correlation

C_p Pressure recovery constant

E	Energy
F	Blending function
g	Gravitational constant
h	Enthalpy
I	Rothalpy
K	Total pressure loss coefficient
k	Kinetic energy
L	Characteristic length scale
M	Mach number
m	Mass
N	Rotational speed
n	Normal vector
P	Pitch
p	Pressure
P_k	Production term
P_R	Rotor Pitch
P_S	Stator Pitch
Q	Heat transfer, Volume flow rate
r	Radius
S	Source term, Swirl coefficient
s	Entropy, Orthogonality vector
T	Temperature
t	Time
U	Blade velocity, Mean velocity
u	Velocity
u_*	Friction velocity
W	Work

y	Wall distance
y^+	Dimensionless wall distance
z	Height

Subscripts

0	Stagnation property, Volute inlet
1	Stator inlet
2	Stator throat
3	Stator outlet
4	Rotor inlet
5	Rotor throat
6	Rotor outlet
7	Diffuser outlet
θ	Tangential direction
i	Isentropic
i,j,k	Direction
R	Rotor
rel	Relative property
S	Stator
t	Turbine, Turbulent
tt	Total-to-Total
w	Relative velocity, Wall

Chapter 1

Introduction

The aim of this thesis is to develop a method to automate the set up process of a CFD simulation and study the flow of a generic fluid radial turbine design. This method could then be used to verify the coherence between an in-house mean line design performance code and 3D CFD simulations in a robust and simple way. The method can also be used as a conceptual design tool for radial turbines and supports most fluids defined in the REFPROP™ software database. REFPROP™ provides tables and plots of the thermodynamic and transport properties of 139 industrially important fluids and their mixtures [1]. To show the capability of the method developed, without going into full analysis with mesh dependent study and as high quality mesh as possible, a comparison is made between the performance code and the 3D CFD simulations. A flow chart of the design process can be seen in Figure 1.1. The process starts with the mean line performance code. A simplified model of the turbine, called Single Blade Passage (SBP) model, gives preliminary results of the three dimensional geometry. In the SBP model only one rotor and stator blade passage is simulated. The SBP can be simulated with or without tip clearance. After the user is satisfied with the performance results from the selected turbine design in the SBP simulation a more comprehensive simulation of a Full Turbine (FT) model can be calculated. The FT model is the final step to verify the radial turbine conceptual design. The turbine analysis is carried out using Computational Fluid Dynamics (CFD) and structural analysis by means of Finite Element Analysis (FEA).

The stresses in the rotor blades are analyzed. One way Fluid Structural Interactions (FSI) are used to map the fluid pressure on the blade surfaces. The stress from centrifugal forces is calculated and investigated if the stress from the fluid pressure or centrifugal forces is dominant.

A number of programs from ANSYS™ are used in the frame of this thesis. The programs are DesignModeler™ and ICEM CFD™ for CAD modeling, TurboGrid™ and ICEM CFD™ for meshing, CFX™ is used as the CFD solver and Mechanical™ for structural analysis.

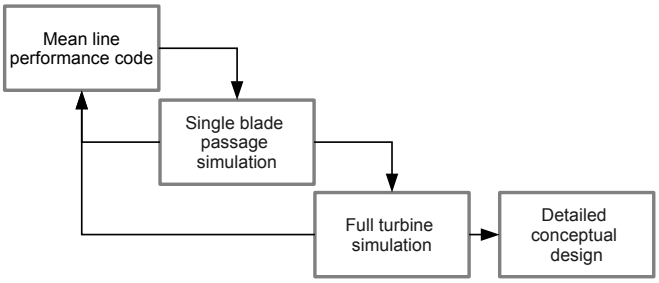

Figure 1.1: Turbine design development

1.1 Background

A Chalmers in-house mean line performance Matlab™ code has been developed and is provided for this project. The mean line design is extended using 3D CFD simulations to obtain a detailed conceptual design tool. The performance code simulates the radial turbine performance based on a given set of variables, i.e. mass flow, specific speed, inlet total temperature, inlet total pressure and the total to total pressure ratio. The performance code calculates the preliminary design of the turbine geometry. The geometry includes the volute, stator and rotor blades and the diffuser, which are given as pointclouds in Cartesian coordinates. The performance code designs the geometry based on a mean line design. The turbine blades are designed at operating conditions under thermal and mechanical stress which is often referred to as hot design. If one would decide to manufacture a turbine the hot design would have to be transferred into a cold design. The cold design would have different shape of blades than the hot design as no loading is assumed in the cold design. When the turbine is at operating conditions the shape would change and match the desired hot design. The boundary conditions, rotational speed, total inlet pressure, total temperature and static outlet pressure are provided for the 3D simulation.

1.2 Purpose

A 3D simulation will give a more realistic result of the flow behavior in the turbine and reveal if the geometry design based on the mean line performance code is reasonable. The flow is expected to have a large Reynolds number and high levels of turbulence. Turbulence is always three dimensional which emphasizes the importance of a full 3D CFD simulation. CFD simulations can give a more detailed result and reveal unexpected flow behavior like separation and shocks. With CFD simulation all properties of the flow can be calculated at any given point, which gives the information for a transient

structural analysis of the blades.

1.3 Radial Turbines

Radial flow turbines are mixed flow turbines, i.e. the flow enters the rotor radially but leaves axially. Flow enters the turbine through a volute. The purpose of the volute is to distribute the flow evenly to the stators. The working fluid is accelerated and turned over the stator blades and is given a circumferential velocity about the rotational axis of the turbine. The flow is turned from radial direction to axial through the rotor with rotor vanes extending radially inward from station 4 in Figure 1.2. The flow exits the turbine axially and is diffused by an exhaust diffuser. The diffuser slows down the flow, recovering some of the static pressure.

Compressible radial flow turbines are small and robust. They have lower mechanical and thermal stress, are lighter and are more efficient due to less tip loss compared to axial turbines of similar power range. Radial turbines are also cheaper than axial turbines due to fewer parts. For higher power ranges ($\sim$ 2 MW) the radial turbine efficiency is similar to axial turbine but gets very heavy and the rotor blades become expensive [2]. Radial turbines are used in a wide range of application, e.g. to power automotive turbochargers, as Auxiliary Power Units (APU) in aircraft and for small power generation units.

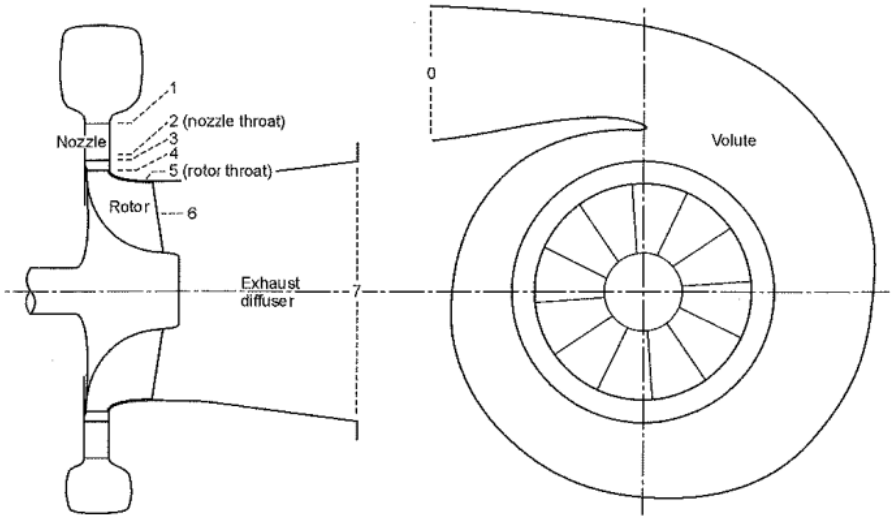

Figure 1.2: Radial inflow turbine [3]

1.4 Limitations

In this chapter the limitations and other simplifications will be described. Several simplifications have been made to both the FT model and the SBP model. The project aim is more methodological than theoretical so in neither case a mesh dependent study has been made. No off-design performance has been evaluated.

1.4.1 Single Blade Passage

Setting up and simulating a full turbine, including the volute and the diffuser, is computationally demanding. It is efficient to have a simplified model that can be set up relatively fast and decrease the simulation time. A way of simplifying the simulation is to simulate only a SBP, i.e. the flow over one stator and one rotor. Simulating the SBP decreases the calculation domain by an order of magnitude. In the SBP the calculation domain is only one stator and one rotor blade and does not include the rest of the blades nor the volute and the diffuser.

Boundary Simplifications in SBP

The simplified SBP model introduces calculation errors at the periodic boundaries since the periodicity has to be modeled. The periodic boundaries are defined on the sides of the stator and rotor passage and the flow exiting one side enters the other. The interface between stator and rotor is modeled since there is a change in frame of reference between rotating and stationary domains. For the SBP only the stator rotor interface has to be modeled since those simulations exclude the volute and the diffuser. One of the main purposes of the volute is to distribute the flow evenly to the stators. This means that the inlet boundary conditions have to be approximated for the SBP since it is hard to evaluate exactly the flow distribution from the volute.

The inlet of the stator domain is comparable to a duct between the volute and the stator in the full turbine model. As there is no volute to distribute the flow the inlet flow angles are defined manually in CFX™. The outlet of the rotor is simplified to extend axially straight from the hub and shroud and does not diverge as a diffuser.

Fluid Structural Interaction

Two way FSI is a coupled analysis between the computational fluid dynamics and structural mechanics. It would give better details of the performance of the turbine but is far greater in complexity than one way FSI. The fluid and structural mesh would depend on each other and would have to be able to deform. Carrying out a two way FSI would exceed the time limit of this project.

Stress Analysis

The structural analysis is performed with the same geometry used in the SBP simulation. The CAD model includes only the blade and not the hub. The blade has sharp edges at the fixed boundaries which lead to stress concentrations, especially at the rotor hub leading edge. This could be avoided by the use of fillets in the rotor hub design.

1.4.2 Full Turbine

The FT model is a much more realistic than the SBP model but still some simplification needs to be applied.

Volute

The volute inlet is simplified to some extent. The Matlab code solves the geometry of the volute piece wise by a single degree. When the circle is completed, the end of the volute has no information about the inlet and thus when the 3D geometry is modeled the end of the volute intersects the inlet. This can be seen in Figure 1.3a. In Figure 1.3b the simplified model of the volute can be seen. In order to focus on building methods for automation of the CFD setup the inlet of the volute is approximated to be shorter than it should be, i.e. it starts at the same location as the volute area goes to zero.

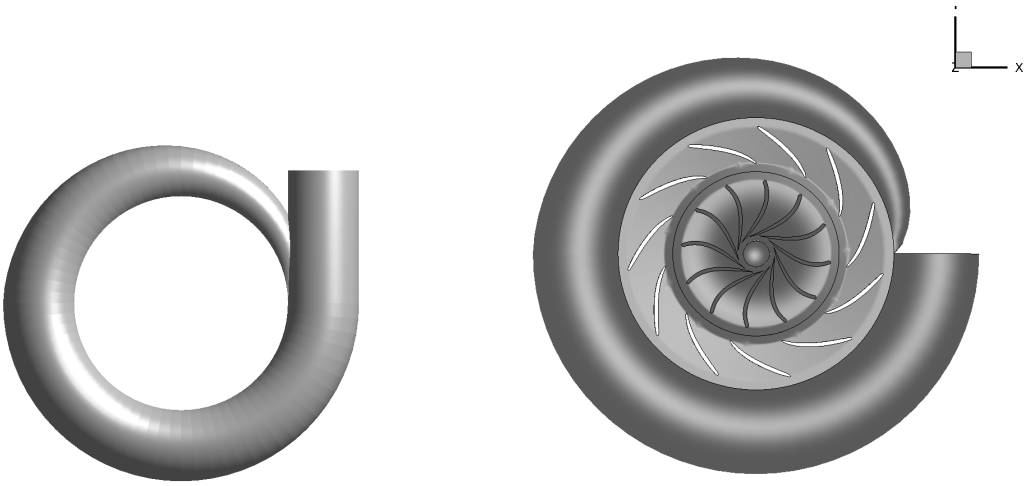

(a) Volute inlet intersection **(b)** Simplified volute

Figure 1.3: Comparison of volutes

Tip clearance

Including tip clearance in the FT model would be very time consuming and would exceed the time limit given in this project. Therefore it has not been considered. The effect has however been considered for the SBP model to assess the effect of the tip clearance.

Chapter 2

Theory

A fundamental understanding of the flow behavior of a radial turbine is necessary to be able to understand the results from the CFD simulation. For the simulation of the radial turbine computer aided calculations are needed. The calculations are divided into two parts, structural analysis and fluid dynamics. The structural analysis is calculated with the FEA approach while the CFD method uses the Finite Volume Method (FVM) for fluid dynamics.

2.1 Radial Turbine Theory

Radial turbines consist of four main components: the volute, the stator, the rotor and the exhaust diffuser. In Figure 2.1 an h-s diagram for the process is shown. Station 0 is at the volute inlet, 1 at the stator or nozzle inlet, 2 at the stator throat, 3 at the stator outlet, 4 at the rotor inlet, 5 at the rotor throat, 6 at the rotor outlet and 7 at the diffuser outlet. The power output of the turbine is generated over the rotor stage, between stations 4 and 6. A geometrical representation can be seen in Figure 1.2.

2.1.1 First Law of Thermodynamics

For an infinitely small change of state the first law of thermodynamics gives [3]:

$$\mathrm{d}E = \mathrm{d}Q - \mathrm{d}W, \tag{2.1}$$

where

$$\mathrm{E} = \mathrm{U} + \frac{1}{2}mc^2 + mgz. \tag{2.2}$$

For a steady state flow it has been shown by Çengel and Boles [5] that Equation 2.1 can be written on the form

$$\dot{Q} - \dot{W}_{\mathrm{x}} = \dot{m}\left[(h_7 - h_0) + \frac{1}{2}\left(c_7^2 - c_0^2\right) + g(z_7 - z_0)\right]. \tag{2.3}$$

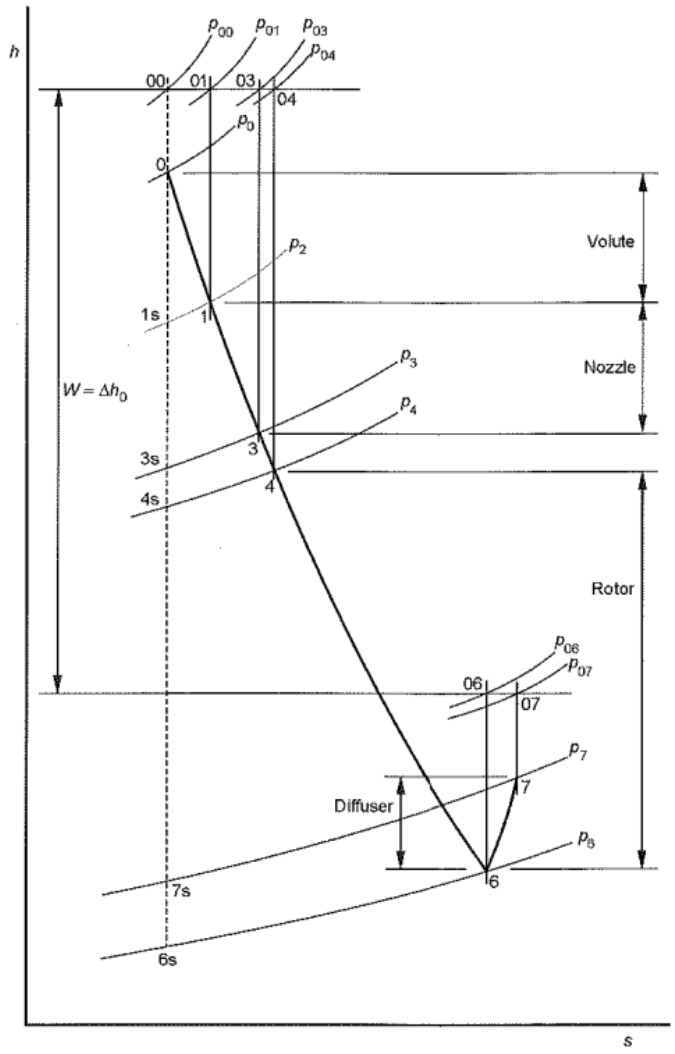

Figure 2.1: h-s diagram of the process of a radial turbine [4]

The contribution from the last term on the right hand side is usually negligible and ignored in gas turbine calculations since the difference in height is minimal. The other two terms are usually rewritten as the stagnation enthalpy,

$$h_0 = h + \frac{1}{2}c^2. \tag{2.4}$$

For most gas turbines the process is close to adiabatic and therefore the first term on the left hand side in Equation 2.3 can be neglected. For a turbine, Equation 2.3 is rewritten:

$$\dot{W}_\mathrm{t} = \dot{m}\left[h_{00} - h_{07}\right]. \tag{2.5}$$

For all components except the rotating parts, there is no work done and therefore the total enthalpy is constant. This gives a constant total enthalpy over each component

except the rotor as seen in Figure 2.1.

For a turbine running at an angular velocity Ω the fluid specific work on the rotor is defined as

$$\frac{\dot{W}_t}{\dot{m}} = \tau_A \Omega = (U_0 c_{\theta 0} - U_7 c_{\theta 7}) . \tag{2.6}$$

Equation 2.6 is called *Euler's turbine equation* [3] and can be rewritten using Equations 2.5 and 2.6:

$$\mathrm{I} = h_0 - U c_\theta \tag{2.7}$$

where I is widely called rothalpy and is constant along streamlines through the turbine. By substituting relative velocity for absolute velocity the relative stagnation enthalpy can be derived. The rothalpy is defined as

$$I = h_{0,rel} - \frac{1}{2} U^2 \tag{2.8}$$

where the relative stagnation enthalpy is defined as

$$h_{0,rel} = h + \frac{1}{2} w^2. \tag{2.9}$$

This property is useful when analyzing the flow of a rotating system like a turbine, since the rothalpy will stay constant through the rotating stage.

A simple form of the isentropic efficiency of the turbine is defined as a function of the enthalpy [3]:

$$\eta_i = \frac{h_{00} - h_{07}}{h_{00} - h_{07s}}. \tag{2.10}$$

2.1.2 Specific Speed

The concept of specific speed can be useful in describing turbomachinery operating requirements. The non-dimensional specific speed is defined [3]

$$\Omega_s = \frac{\Omega Q^{1/2}}{\triangle h_{0s}^{3/4}} \tag{2.11}$$

where Ω is the shaft speed, $\triangle h_{0s}$ is the total to total enthalpy drop and Q is the flow rate at the rotor exit [6].

The specific speed can be used to characterize the general form or shape of the turbine and is also known as a shape factor. The specific speed can be used to identify the region for the best efficiency for a radial turbine. As seen in Figure 2.2 the best efficiency will be obtained in the range of $0.3 < \Omega_s < 0.8$ for air. This is the range where a radial turbine can be favorable compared to an axial turbine as axial and radial turbines in this range deliver very similar efficiency. The specific speed is independent of the size of the turbine and can therefore be used to scale up or down a geometrically similar turbine without changing the turbine efficiency [4].

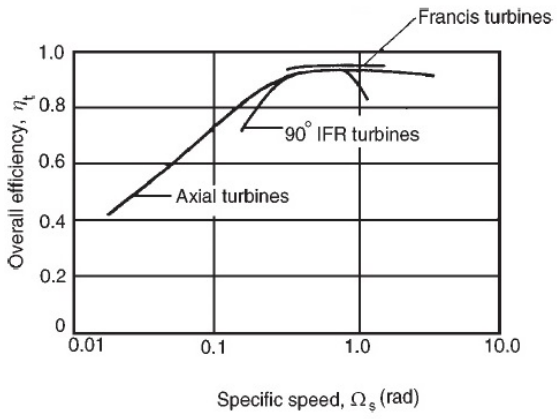

Figure 2.2: Overall efficiency as a function of the specific speed for comparison of axial turbines and inward-flow radial turbines [3]

2.1.3 Blade Passage Losses

To maximize the turbine efficiency it is necessary to minimize the losses. There are four major losses in a radial turbine stage. In Figure 2.3 the rotor losses as a function of the incidence are shown [7].

Channel Loss

Channel loss represents the skin friction between the fluid and the endwall surfaces. Channel losses are mainly dependent on the surface finish and component geometry. For the rotating components, they are also dependent on the relative velocity ratio of the rotor outlet over the rotor inlet, w_6/w_4.

Incidence Loss

For nonzero incidence the flow will not follow the ideal streamline leading to additional losses at the leading edge. This is called shock or incidence losses but it has nothing to do with shock waves. Figure 2.3 shows how rapidly the shock losses increase when the incidence deviates from zero degrees.

Secondary Loss

Secondary loss is due to the secondary flow vortices generated by the shape of the passage and the boundary layers. Because of this a part of the fluid moves in another direction than the main flow. Consider a blade passage like the one in Figure 2.4. The vortices from the channel boundary layer are split at the leading edge, one part to the pressure side and the other to the suction side. The one that goes to the pressure side gets sucked to the suction side of the adjacent blade creating passage vortex. This also happens to the boundary layer on the pressure side creating the endwall crossflow. The other

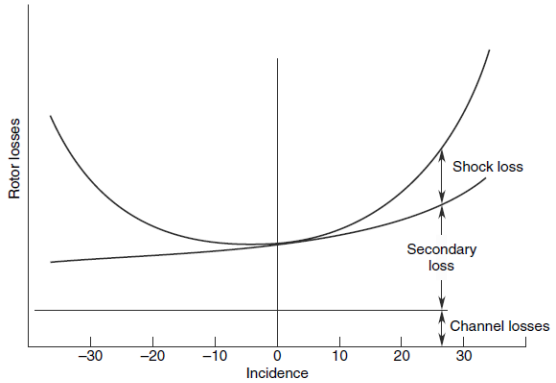

Figure 2.3: Losses of a radial turbine stage as a function of incidence [7]

vortex, the one on the suction side from the leading edge, is called counter vortex. It is called counter vortex since it is counter rotating to the one that is sucked to the suction side. This fluid behavior creates the 3D wake downstream of the blades. From this the loss is increased through viscous shear and fluid mixing.

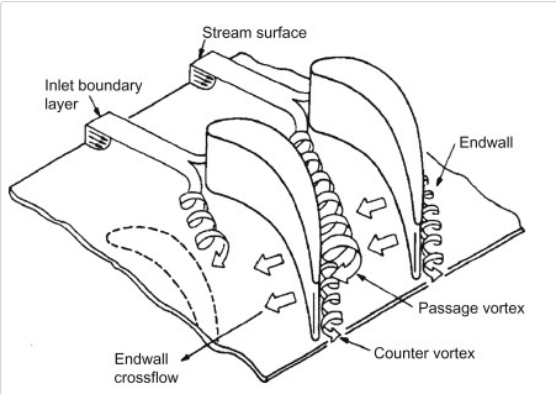

Figure 2.4: Vorticity generation in a blade passage [7]

Tip Leakage

Tip clearance is necessary between the rotor and the shroud for the rotor not to intersect when the turbine is expanded by thermal and centrifugal forces. As a result of the tip clearance, leakage occurs between the pressure side and the suction side of the blades, causing loss. The tip clearance can have a significant effect on the turbine efficiency.

Tip leakage is a loss parameter that is not dependent on the incidence but rather on the relative size of the tip clearance compared to the blade height. The fluid that goes through the clearance does not contribute to the work done on the rotor by the fluid, i.e.

the work output of the turbine will become lower compared to ideal conditions. Because of the different velocities of the blades and the shroud wall, vortices are formed. They interact with the vortices mentioned previously in secondary losses. Together they are creating very complex flows which will lead to increased losses. The efficiency is much more sensitive to the radial than the axial tip clearance as most of the energy from the flow is extracted in the exit area of the rotor blade [8].

2.1.4 Volute

The purpose of the volute is to distribute the flow evenly to the stator blades. This is to ensure that each of the rotor blade will receive an equal amount of massflow, i.e. the rotor blades will be evenly loaded. The flow is uniform at the volute inlet, it is assumed to come from a straight pipe. The preliminary design is based on the assumption that the angular momentum is constant, described by the free vortex equation:

$$rC_\theta = \text{constant} \tag{2.12}$$

and the continuity equation in the θ direction

$$m_\theta = \rho_\theta A_\theta C_\theta. \tag{2.13}$$

For a more realistic preliminary design of the volute some loss terms [4] can be introduced in Equations 2.12 and 2.13 [4]. In the continuity equation a blockage term, B, is included to account for the effects of boundary layer and secondary flow. The continuity equation can then be presented on the form:

$$m = \rho_1 A_1 (1 - B_1) C_1. \tag{2.14}$$

The effects from the wall friction can be accounted for by introducing a total pressure loss coefficient, K, and a swirl coefficient, S, in the free vortex equation:

$$K = \frac{p_{00} - p_{01}}{p_{01} - p_1} \quad \text{and} \quad r_1 C_{1\theta} = S r_0 C_0. \tag{2.15}$$

By including these factors in equations 2.12 and 2.13 the volute design ought to be more accurate and give better results in CFD simulations.

2.1.5 Stator

The stator rows guide and accelerate the flow to the rotor blades. Losses in the stator can be represented as a total pressure loss coefficient. The loss coefficient is defined as [4]

$$\frac{p_{01} - p_{03}}{p_{03} - p_3}. \tag{2.16}$$

Hiett and Johnston [9] recommend that the pressure loss coefficient should be in the range of $0.03 - 0.07$ for the stator passage. If the volute is included the loss coefficient should be in the range of $0.05 - 0.13$.

2.1.6 Rotor

The energy is extracted from the flow in the rotor. To maximize the work output from the turbine the losses have to be minimized. According to Baines [4] the channel and secondary losses can be modeled with the profile length defined as

$$L_P = K_P \left\{ \left(\frac{L_H}{D_H} \right) + 0.68 \left[1 - \left(\frac{\overline{r}_5}{r_4} \right)^2 \right] \frac{\cos(\beta_{b5})}{(b_5/c)} \right\} \frac{1}{2} \left(W_4^2 + W_5^2 \right). \tag{2.17}$$

The hydraulic length L_H is defined

$$L_H = \frac{\pi}{4} \left[\left(z - \frac{b_4}{2} \right) + \left(r_4 - r_{5t} - \frac{b_5}{2} \right) \right] \tag{2.18}$$

and the hydraulic diameter D_H

$$D_H = \frac{1}{2} \left[\left(\frac{4\pi r_4 b_4}{2\pi r_4 + Z_R b_4} \right) + \left(\frac{2\pi \left(r_{5t}^2 - r_{5h}^2 \right)}{\pi \left(r_{5t} - r_{5h} \right) + Z_R b_5} \right) \right]. \tag{2.19}$$

The coefficient K_P is equal to 0.11. A correction of turbines with high specific speeds is necessary and then the coefficient is multiplied with a factor of 2. This multiplication is needed when

$$\frac{r_4 - r_{5t}}{b_5} < 0.2. \tag{2.20}$$

The tip clearance losses can be modeled with the clearance length L_C which according to Baines [4] is defined as

$$L_C = \frac{U_4^3 Z_R}{8\pi} \left(K_x \varepsilon_x C_x + K_r \varepsilon_r C_r + K_{xr} \sqrt{\varepsilon_x \varepsilon_r C_x C_r} \right) \tag{2.21}$$

where

$$C_x = \frac{1 - (r_{6t}/r_4)}{C_{m4} b_4} \tag{2.22}$$

and

$$C_r = \left(\frac{r_{6t}}{r_4} \right) \frac{z - b_4}{C_{m6} r_6 b_6}. \tag{2.23}$$

The coefficients values $K_r = 0.75$, $K_x = 0.4$ and $K_{xr} = -0.3$ have shown good coherence with experimental data [4].

2.1.7 Exhaust Diffuser

The exhaust diffuser is an important component for the performance of a radial turbine. In the exhaust diffuser the flow is slowed down recovering some of the static pressure through recovery of kinetic energy. At the turbine exit the pressure must recover to the ambient pressure. With the diffuser, a lower pressure at the rotor exit (station 6 in

Figure 2.1) can be reached. This allows for more work to be extracted from the rotor resulting in higher efficiency.

The pressure recovery is measured through the pressure recovery constant which is defined [4]

$$C_p = \frac{p_7 - p_6}{p_{06} - p_6}. \tag{2.24}$$

The main problem when designing the diffusers is the risk of boundary layer separation at the wall. When the diffusion angle θ, seen in the top left corner in Figure 2.5, is large the diffusion rate is rapid and can cause boundary layer separation resulting in flow mixing and stagnation pressure losses. On the other hand if the diffusion rate is too low, the required length of the diffuser will be very large and the fluid friction losses increase [3].

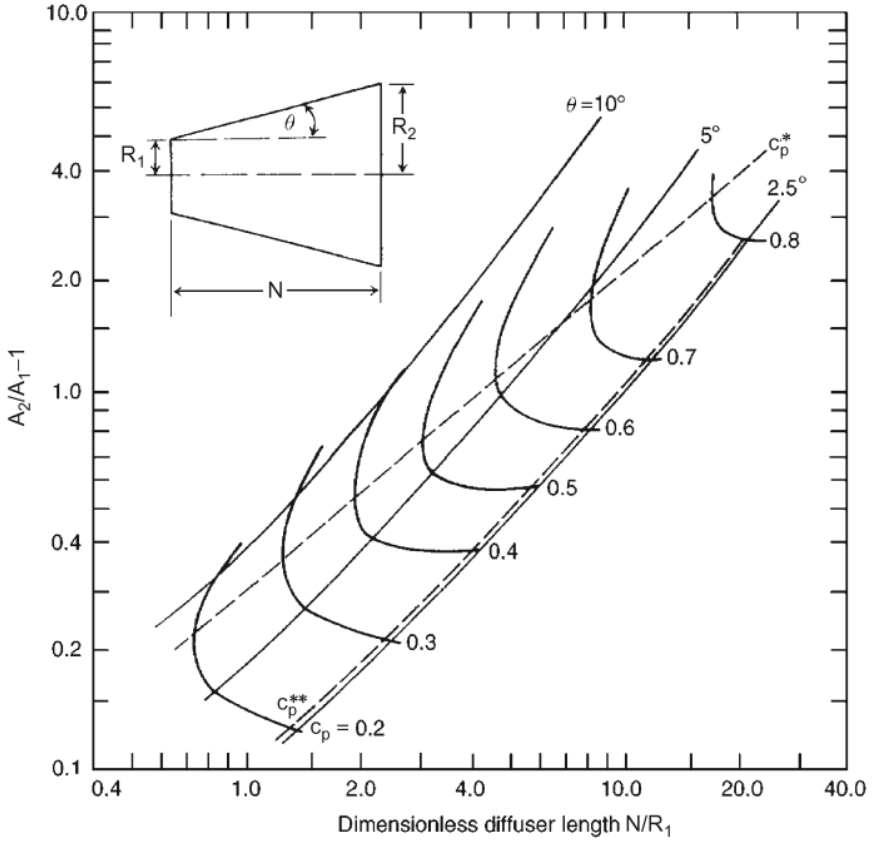

Figure 2.5: Diffuser geometry and performance [3]

The upper dashed line in Figure 2.5, C_p^*, and the one below, C_p^{**}, represent optimum diffuser lines plotted on diffuser performance data presented by Sovran and Klomp [10]. C_p^* is the locus of points that defines the diffuser area ratio producing the maximum

pressure recovery for a prescribed nondimensional length. C_p^{**} is the locus of points defining the diffuser nondimensional length, producing the maximum pressure recovery at a prescribed area ratio [3].

2.2 Computational Fluid Dynamics

The results of a CFD simulation are highly dependent on the models and the methods that are specified when setting up the simulation. Therefore it is important to choose the ones that give high accuracy along with minimum computational cost. Solving the Navier-Stokes equations, Reynolds Averaged Navier Stokes (RANS) is used for steady simulation and Unsteady Reynolds Averaged Navier Stokes (URANS) for transient. The SST $k-\omega$ turbulence model is used due to its ability to switch between the $k-\varepsilon$ and $k-\omega$ model and in order to combine the most accurate range of each model. At this stage of the design, RANS is suitable as it is much less computationally expensive than other models such as LES.

2.2.1 Governing Equations

The governing equations to resolve the flow field are the continuity equation, the momentum equation and the energy equation. The momentum equation is also known as the Navier-Stokes equation. Those three equations together are also often referred to as the Navier-Stokes equations and are presented below on their conservation form for compressible ($\frac{\partial u_i}{\partial x_i} \neq 0$) flow. The continuity equation reads:

$$\frac{\partial \rho}{\partial t} + \frac{\partial (\rho u_i)}{\partial x_i} = 0. \tag{2.25}$$

The momentum equation can be written:

$$\frac{\partial (\rho u_i)}{\partial t} + \frac{\partial (\rho u_i u_j)}{\partial x_j} = -\frac{\partial p}{\partial x_i} + \frac{\partial \tau_{ij}}{\partial x_j} + S_M \tag{2.26}$$

where the stress tensor τ is related to the strain rate by:

$$\tau_{ij} = \mu \left[\left(\frac{\partial u_i}{\partial x_j} + \frac{\partial u_j}{\partial x_i} \right) - \frac{2}{3} \delta_{ij} \frac{\partial u_j}{\partial x_i} \right] \tag{2.27}$$

and the total energy equation reads:

$$\frac{\partial (\rho h_{tot})}{\partial t} - \frac{\partial p}{\partial t} + \frac{\partial (\rho u_j h_{tot})}{\partial x_j} = \frac{\partial}{\partial x_j} \left(\lambda \frac{\partial T}{\partial x_j} \right) + \frac{\partial (u_i \tau_{ij})}{\partial x_j} + \boldsymbol{S}_E \tag{2.28}$$

where S_E and S_M are source terms. The source terms either produce or dissipate energy or momentum.

The Navier Stokes equations are transformed to the RANS equations by decomposing

the instantaneous velocity to a mean and fluctuating component. This decomposition gives an extra term that is unknown, called the Reynolds stress. The Reynolds stress is modeled using a turbulence model, commonly an eddy viscosity model or Reynolds Stress Model (RSM).

2.2.2 Turbulence Model

SST $k-\omega$ turbulence model is a two equation eddy viscosity turbulence model which is suggested for flow with adverse pressure gradients [11]. Considering the suction side of a blade, the pressure decreases as the velocity increases when the flow hits the leading edge of the blade. The pressure reaches a local minimum at the crest of the blade and starts to increase again, leading to an adverse pressure gradient for the flow, i.e. $\frac{dp}{dx} > 0$.

In such flows, the standard $k-\varepsilon$ model overpredicts the level of turbulent shear stress because of too large length scale [12]. The $k-\varepsilon$ model is less sensitive to the free stream value turbulence properties while the $k-\omega$ model tends to depend on free-stream turbulence properties. The $k-\omega$ model does not require any damping functions while the $k-\varepsilon$ requires complex nonlinear damping functions for near wall-modifications.

Since the two models have different strengths and weaknesses, a hybrid model was developed by Menter [13] to combine the most accurate regimes of the two models. That resulted in the two equation eddy viscosity SST $k-\omega$ model. In the model, the $k-\omega$ model is used in the near wall region and transforms to a $k-\varepsilon$ far from the wall in the fully turbulent region. With the ability to combine the strengths of the $k-\omega$ and the $k-\varepsilon$ respectively, the SST $k-\omega$ becomes an appropriate choice for adverse pressure gradients.

The k equation in Wilcox's [14] two equation $k-\omega$ model reads:

$$\frac{\partial(\rho k)}{\partial t} + \frac{\partial(\rho U_j k)}{\partial x_j} = \frac{\partial}{\partial x_j}\left[\left(\mu + \frac{\mu_t}{\sigma_{k1}}\right)\frac{\partial k}{\partial x_j}\right] + P_k - \beta^*\rho k\omega \tag{2.29}$$

and the ω equation:

$$\frac{\partial(\rho\omega)}{\partial t} + \frac{\partial(\rho U_j \omega)}{\partial x_j} = \frac{\partial}{\partial x_j}\left[\left(\mu + \frac{\mu_t}{\sigma_{\omega 1}}\right)\frac{\partial \omega}{\partial x_j}\right] + \alpha_1\frac{\omega}{k}P_k - \beta_1\rho\omega^2. \tag{2.30}$$

The turbulent viscosity is defined

$$\nu_t = \frac{\mu_t}{\rho} = \frac{k}{\omega} \tag{2.31}$$

and the Reynolds stresses in the production term P_k are calculated using the Boussinesq assumption, i.e. turbulent viscosity is introduced to model the Reynold's stresses:

$$-\overline{u_i' u_j'} = \nu_t\left(\frac{\partial U_i}{\partial x_j} + \frac{\partial U_j}{\partial x_i}\right) - \frac{2}{3}\delta_{ij}\left(k + \nu_t\frac{\partial U_k}{\partial x_k}\right). \tag{2.32}$$

The $k-\varepsilon$ is transformed to a $k-\omega$ model using the turbulence frequency, defined $\omega = \varepsilon/k$, as a second variable and the length scale is $l = \sqrt{k}/\omega$. The k equation in the transformed $k-\varepsilon$ model reads:

$$\frac{\partial(\rho k)}{\partial t} + \frac{\partial(\rho U_j k)}{\partial x_j} = \frac{\partial}{\partial x_j}\left[\left(\mu + \frac{\mu_t}{\sigma_{k2}}\right)\frac{\partial k}{\partial x_j}\right] + P_k - \beta^*\rho k\omega \tag{2.33}$$

and the ω equation

$$\frac{\partial(\rho\omega)}{\partial t} + \frac{\partial(\rho U_j \omega)}{\partial x_j} = \frac{\partial}{\partial x_j}\left[\left(\mu + \frac{\mu_t}{\sigma_{\omega 2}}\right)\frac{\partial \omega}{\partial x_j}\right] + 2\rho\frac{1}{\sigma_{\omega 2}\omega}\frac{\partial k}{\partial x_j}\frac{\partial \omega}{\partial x_j} + \alpha_2\frac{\omega}{k}P_k - \beta_2\rho\omega^2. \tag{2.34}$$

The k equation in the standard SST $k-\omega$ model, with buoyancy term disregarded, reads:

$$\frac{\partial(\rho k)}{\partial t} + \frac{\partial}{\partial x_j}(\rho U_j k) = \frac{\partial}{\partial x_j}\left[\left(\mu + \frac{\mu_t}{\sigma_{k3}}\right)\frac{\partial k}{\partial x_j}\right] + P_k - \beta^*\rho k\omega, \tag{2.35}$$

where the production term is defined

$$P_k = \left(2\nu_t s_{ij} s_{ij} - \frac{2}{3}k\frac{\partial v_i}{\partial x_j}\delta_{ij}\right). \tag{2.36}$$

The ω equation reads

$$\frac{\partial(\rho\omega)}{\partial t} + \frac{\partial}{\partial x_j}(\rho U_j \omega) = \frac{\partial}{\partial x_j}\left[\left(\mu + \frac{\mu_t}{\sigma_{\omega 3}}\right)\frac{\partial \omega}{\partial x_j}\right] + (1-F_1)2\rho\frac{1}{\sigma_{\omega_2}\omega}\frac{\partial k}{\partial x_j}\frac{\partial \omega}{\partial x_j} + \alpha_3\frac{\omega}{k}P_k - \beta_3\rho\omega^2 \tag{2.37}$$

where the blending function F_1 is defined as

$$F_1 = \tanh(\xi^4) \tag{2.38}$$

with

$$\xi = \min\left[\max\left\{\frac{\sqrt{k}}{\beta^*\omega y}, \frac{500\nu}{y^2\omega}\right\}\frac{4\rho k}{CD_{k\omega}\sigma_{\omega 2}y^2}\right] \tag{2.39}$$

and

$$CD_{k\omega} = \max\left\{2\rho\frac{1}{\sigma_{\omega 2}\omega}\frac{\partial k}{\partial x_j}\frac{\partial \omega}{\partial x_j}, 1\cdot 10^{-10}\right\}. \tag{2.40}$$

The turbulent viscosity is defined

$$\nu_t = \frac{a_1 k}{\max(a_1\omega, SF_2)} \tag{2.41}$$

and

$$F_2 = \tanh(\eta^2) \tag{2.42}$$

with

$$\eta = \max\left\{\frac{2k^{1/2}}{\beta^*\omega y}, \frac{500\nu}{y^2\omega}\right\}. \tag{2.43}$$

Using a blending function the model transforms from a $k-\omega$ model to a $k-\varepsilon$ model. Near the wall, $F_1 = 1$, the model behaves as a $k-\omega$ model but far from the wall, $F_1 = 0$, the model behaves as a $k-\varepsilon$ model. The variable y is defined as the distance to the closest wall node. The constants are a linear combination, $\Phi_3 = F_1\Phi_1 + (1-F_1)\Phi_2$, of the coefficients of the $k-\omega$ and $k-\varepsilon$ models and are defined:

$$\begin{aligned}
&\beta^* = 0.09,\\
&\alpha_1 = 5/9\\
&\beta_1 = 0.075,\\
&\sigma_{k1} = 2,\\
&\sigma_{\omega 1} = 2,\\
&\alpha_2 = 0.44,\\
&\beta_2 = 0.0828,\\
&\sigma_{k2} = 1,\\
&\sigma_{\omega 2} = 1/0.856.
\end{aligned}$$

2.2.3 Fluid Domain Mesh

The mesh of the fluid domain has to be of high quality to have faster convergence and to capture the flow characteristics. To resolve the boundary layer the y^+ value has to be chosen with respect to the turbulence model.

Fluid Mesh

In Figure 2.6 and Table 2.1 the quality criteria for the CFX™ solver is specified. The figure shows how the angle for the quadrilateral faced element is not as good as it could be. The normal vector for the integration point surface, n, and the vector that joins two control volume nodes, s, are not parallel. However for the triangular faced element the orthogonality is of highest order since the vectors are parallel. The best measurement on the mesh orthogonality is the orthogonality angle which is the area weighted average of $90°-\text{acos}(n \cdot s)$. According to Table 2.1 the area weighted average of the orthogonality angle can not be smaller than 20° but local angles can be as low as 10°.

Wall distance

The wall distance y is calculated with following equations. The Reynolds number is defined:

$$Re = \frac{\rho \cdot U_{\text{FreeStream}} \cdot L_{\text{BoundaryLayer}}}{\mu} \tag{2.44}$$

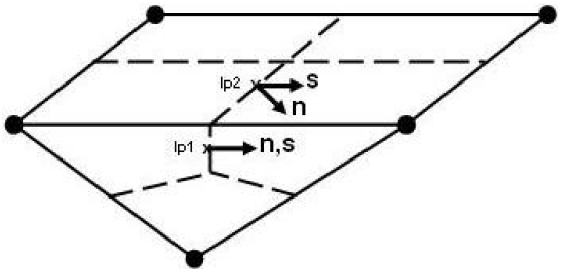

Figure 2.6: Orthogonality for quadrilateral and triangular faced elements

Table 2.1: CFX™ mesh quality criteria [15]

Measure	Acceptable Range	Description
Orthogonality angle	$> 20°$	Area weighted average of $90° - \text{acos}\,(n \cdot s)$
Orthogonality factor	$^1/_3$	Area weighted average of $n \cdot s$
Orthogonality angle minimum	$> 10°$	Minimum of $90° - \text{acos}\,(n \cdot s)$
Orthogonality factor	$^1/_6$	Minimum of $n \cdot s$
Minimum and maximum face angle	$> 10°$ and $< 170°$	Minimum and maximum angle between edges of each face
Minimum and maximum dihedral angle	$> 10°$ and $< 170°$	Minimum and maximum angle between element faces

where ρ is the fluid density, μ the kinematic viscosity, $U_{\text{FreeStream}}$ is the characteristic velocity and $L_{\text{BoundaryLayer}}$ is the characteristic length scale. The skin friction is defined according to White skin friction correlation [16]

$$C_{\text{f}} = 0.027 Re_x^{-1/7}. \tag{2.45}$$

The wall shear stress is then defined as

$$\tau_{\text{w}} = C_{\text{f}} \cdot \frac{1}{2} \rho U_{\text{FreeStream}}^2 \tag{2.46}$$

and the friction velocity

$$u_* = \sqrt{\frac{\tau_{\text{w}}}{\rho}}. \tag{2.47}$$

The element size at the wall in the wall normal direction is calculated:

$$y = \frac{y^+ \mu}{\rho u_*}. \tag{2.48}$$

The wall distance is directly related to the dimensionless wall distance y^+ which is defined by the turbulence model. For the SST $k - \omega$ model, the near wall element y^+ value is

within the log-law region, in the range of 30-300. Keeping the y^+ in this range should capture the most important flow behavior with acceptable mesh resolution and short simulation time.

2.2.4 CFX™ - Setup

In CFX™ there are few important models that have to be studied for the most accurate and least computational demanding simulation. The interfaces at the rotor inlet and outlet are important since the flow properties are transformed between the mesh domains for both the steady state and the transient case. For the SBP transient case the number of blade passages to be simulated is dependent on the models and also the disturbances from the upstream domain are handled.

Automatic Wall Function

For treatment of the flow near the wall two approaches are available: either the wall function or the Low-Reynolds-Number method, the latter is in this case the $k-\omega$ model.

The wall function uses algebraic equations with a turbulence model, which is valid for the $k-\varepsilon$ model, to account for the viscous sublayer instead of resolving the boundary layer saving computational resources. However this can create inaccuracy when the near wall elements are inside the viscous sublayer, i.e. the center of the near wall elements is too close to the wall, $y^+ < 11.06$.

The Low-Reynolds-Number method is used to be able to resolve the boundary layer accurately. This comes with additional computational cost.

For maximum accuracy and minimum computational cost, the so called automatic wall function switches between the wall function method and the Low-Reynolds-Number method automatically to account for refinement of the mesh. This is very practical in industrial simulations since the right y^+ value can be hard to predict. When the near wall element has a $y^+ > 11.06$ the wall function is used but when $y^+ < 11.06$ the Low-Reynolds-Number method is used. As discussed previously in Chapter 2.2.2 the SST $k-\omega$ model uses a smoothing function to switch between the two methods [15].

Mixing Model

Since the rotor is spinning compared to other parts of the turbine a model is needed for the interfaces between the rotor towards the upstream (stator) as well as towards the downstream (diffuser) components. For the steady case there are two models available in CFX™ but for the transient case there is only one model. The mixing models are:

- Frozen Rotor - Steady state

- Stage (Mixing plane) - Steady state
- Transient Rotor Stator (Sliding interface) - Transient

For the Frozen Rotor and the Transient Rotor Stator interfaces the unequal pitch ratio is accounted for by scaling the flow with the pitch ratio. The pitch ratio is the ratio of the width of the stator blade domain outlet over the rotor blade domain inlet. The unequal pitch is not important for the Stage interface since the fluxes are circumferentially averaged [15].

The Frozen Rotor model treats both frames as stationary which implies that it is dependent on the fixed location of the two frames. A frame transformation is used to represent the rotation of the rotor frame. It is most applicable when the circumferential variation of the flow is large relative to the component pitch since the true flow is transformed between domains. The Frozen Rotor is the least computationally demanding of the three models but also provides the lowest accuracy. The model is a good initial guess for Transient Rotor Stator model and also the Stage model in case the mesh has many elements [15].

In the Stage model, also called Mixing Plane model, the rotor frame is rotating, unlike the Frozen Rotor model. The flow property fluxes are circumferentially averaged upstream of the interface to obtain the boundary conditions for the downstream component. This is called mixing plane interface. As an effect of the circumferential averaging all transient behavior of the flow is averaged out and the inlet boundary conditions for the downstream interface are steady. This results in higher accuracy for flows with small circumferential variations. The Stage model is more computationally demanding compared to the Frozen Rotor model [15].

In the Transient Rotor Stator model the true transient interaction between components is resolved for maximum accuracy for the SBP model or the FT model. This is the same method as the Frozen Rotor model but the relative rotation is also taken into account. This model can be used for the same interfaces as used in the Frozen Rotor and Stage models [15].

For the Frozen Rotor and the Transient Rotor Stator interfaces the unequal pitch ratio is accounted for by scaling the flow with the pitch ratio. The unequal pitch is not important for the Stage interface since the fluxes are circumferentially averaged [15].

Transient Blade Row Modeling

To simulate the transient flow in a reduced domain, either a single blade passage or a number of passages, it is necessary to model the periodic interfaces at the sides of the domains. Some models require pitch ratio close to unity and a minimum of two blade

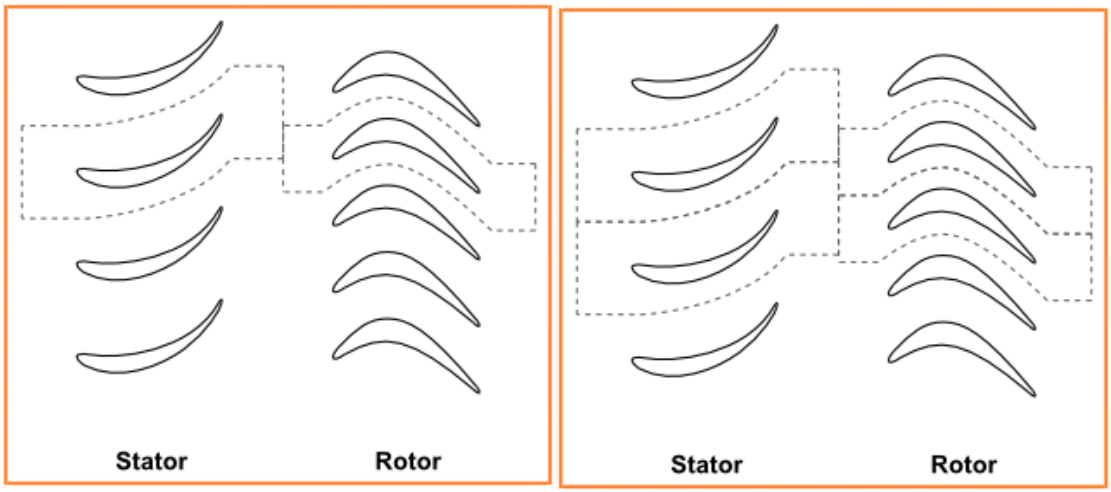

(a) Single blade passage is needed for Time Transformation model

(b) At least two blade passages are needed for Fourier Transformation model

Figure 2.7: Schematic sketch of the transient blade row models

passages to be modeled. This is accomplished by using one of the Transient Blade Row models available in CFX. The included models are:

- Profile Transformation
- Time Transformation
- Fourier Transformation

The Profile Transformation model has to have a pitch ratio between the stator and the rotor close to unity. This can result in a full turbine simulation since many turbines have prime number of blades.

The Time Transformation model is capable of simulating one blade passage, see Figure 2.7a and can be used when the pitch ratio deviates from unity as long as it falls within the range

$$1 - \frac{M_\omega}{1 - M_\theta} < \frac{P_S}{P_R} < 1 + \frac{M_\omega}{1 + M_\theta} \tag{2.49}$$

where M_ω is the Mach number associated with the rotor rotational speed, M_θ is the Mach number associated with the tangential Mach number of the flow and P_R and P_S the pitch of rotor and stator. Giles [17] showed that the pitch ratio can be in the range of 0.6-1.5, where M_ω is in the range of 0.3-0.6. This is the case for most compressible turbomachinery flow [18].

The Fourier Transformation model has no limitation on pitch ratio but two blade passages as seen in Figure 2.7b need to be modeled to capture the periodicity of the domain.

Time Transformation and Fourier Transformation are based on phase shifted periodic conditions. This means that the rotor and stator sides are periodic boundaries at different instances in time. Both models can model rotational flow boundary disturbances.

Disturbance settings

For the disturbances to flow through the interface between the stator and rotor two different options are available [18].

- Rotor Stator
- Rotational Flow Boundary Disturbance

The Rotor Stator option can only be used when the interface is modeled with the Transient Rotor Stator model and the previous stage is simulated and not modeled.

The Rotational Flow Boundary Disturbance option can be used both with steady and transient models. The wake from the upstream blades can be prescribed with a CFX Expression Language (CEL) or external .csv file. This has the possibility to act as a virtual blade row before or after the fluid mesh representing a multi-stage turbomachine. When all stages of a turbine are simulated this option has no application.

2.3 Structural FEA

FEA analysis is used to determine the stress of the blades.

2.3.1 von Mises Criterion

To estimate the strength of the blades the von Mises criterion is used. The von Mises stress is calculated by combining complex 3D loading of normal and shear stress to a single scalar (also known as single, effective, equivalent stress et cetera), that can be compared to the materials yield strength, typically obtained from a uniaxial tension test. If the maximum value of the von Mises stress is higher than the yield strength of the material, the criteria predicts the design will fail. The von Mises stress expressed in terms of the principal stresses is [19]:

$$\frac{1}{2}\left(\sigma_1 - \sigma_2\right)^2 + \left(\sigma_2 - \sigma_3\right)^2 + \left(\sigma_3 - \sigma_1\right)^2 \leq \sigma_y^2 \tag{2.50}$$

2.3.2 Structural Domain Mesh

The mesh depends on the blades and a mesh dependent study should be made to determine sufficient number of elements or element size.
The different types of elements for the 3D structural mesh can be seen in Figure 2.8,

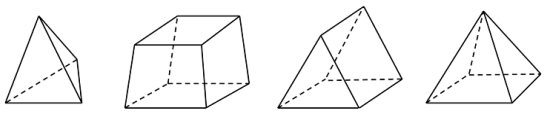

Figure 2.8: Different types of elements in FEA, tetrahedral-, hexahedral-, prism- and pyramid elements repectively.

tetrahedral-, hexahedral-, prism- and pyramid elements, respectively. The most general element is the tetrahedron (first from left) as it can be used to mesh any shape of a 3D object. Using hexahedral and prisms can significantly reduce calculation time; it also involves lower skewness and fewer numerical errors. These elements can have high aspect ratios and therefore reduce the total number of elements in the model.

A combination of the elements is possible. The pyramid elements are used to stitch the tetrahedral elements to the brick or prism elements.

Chapter 3

Methodology

To automate the simulation procedure a set of suitable software is needed. The programs have to support macros or scripting with the capability of automizing the work flow. A script or a macro is defined as "a single instruction that expands automatically into a set of instructions to perform a particular task" [20]. The software used in the frame of this thesis along with its application can be seen in Table 3.1. In this chapter the procedure in each software will be described and motivated why this software is chosen. Two comparison cases are used to compare the CFD simulation to the performance code.

Table 3.1: Definition on which software is used and for what application

Software	Application
Matlab™	Export of data from performance code to 3D geometry
DesignModeler™	3D geometry, SBP
TurboGrid™	Fluid mesh, SBP
ICEM CFD™	3D geometry & fluid mesh, FT
CFX™	CFD simulation
Mechanical™	Structural mesh & FEA simulations, SBP

3.1 Comparison Cases

Two radial turbine cases are used to verify the performance code and design assumptions. The NASA case is based on an experimental study performed in 1966 [21]. The main difference between the turbine in the report and the turbine that is used in this thesis is the number of blades and the stator rotor intersection. The number of blades in the

original report is 14 stator blades and 11 rotor blades, but the turbine used in this thesis has 11 stator blades and 12 rotor blades. The intersection between the stator and rotor is larger than in the experimental study. The NASA report is a performance evaluation of a 6.02 inch radial turbine for Argon fluid. The performance of the NASA turbine is evaluated only over the stator and rotor in the report. The second case is an Organic Rankine Cycle (ORC) radial turbine. The preliminary design results from Sauret and Gu [22] are used in the performance code to generate a conceptual geometry design of the turbine. In the ORC report the performance is evaluated without a volute. The working fluid for the ORC case is refrigerant R143a.

3.2 Performance Code Modifications

The performance code has to be adjusted for exporting the type of data accepted by the software used in the framework of this project.

- Volute
  - In the performance code the area of the volute is calculated assuming a circular cross sectional area. Circular cross section is chosen for simplicity but a more advanced cross section can be used. Examples of volute cross sectional shapes can be seen in Figure 3.1.

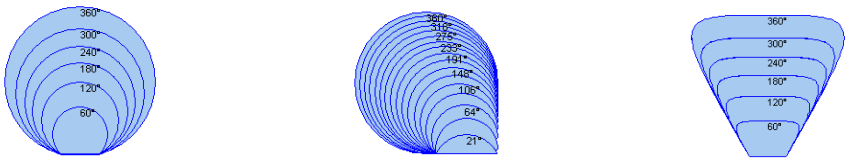

(a) Circular **(b)** Asymmetric **(c)** Trapezoidal

Figure 3.1: Different types of cross section for the volute [23]

  - The outlet of the volute is assumed to be vertical with at least the same height as the leading edge of the stator blade as seen in Figure 3.2.
  - The performance code assumes that the stator is positioned right after the volute with no intermediate duct. This is not practical since the flow will separate at the sharp edge. Instead a duct is placed between the volute and stator as shown in Figure 3.2.
  - The circular cross sectional area of the volute is designed to go to an infinitesimal small area at the end of the volute in the performance code. This is difficult and time consuming to mesh, therefore the end is simplified to an inclined wall instead of a circular cross section. The simplifications apply only to the last 5° degrees of the volute.

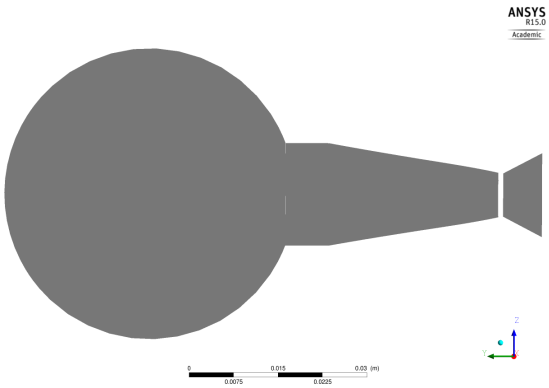

Figure 3.2: Cross section of the volute and stator

- When the turbine design is updated, a Matlab™ script modifies an existing script for the SBP and the FT models. The existing scripts will be adjusted to the new design and ensure that the process is as automated as possible.
- Rotor and stator blade height
  - The blade geometry is created from the camberlines in the performance code according to a method detailed by Aungier [24]. The blades are tilted resulting in higher pressure side than suction side of the blades in 3D. The blade geometry straight from the performance code can be seen in Figure 3.3. The blade is marked 2 and the fluid domain is marked 1. The fluid domain is created using the camber lines. The blade exceeds the fluid domain at the pressure side but the suction side is inside the domain. In order to create an acceptable fluid domain mesh both the rotor and the stator blades are extended at the hub and the shroud. The camber lines at the hub and shroud are then used to slice the extended blades to create blades that intersect the fluid mesh domain both at pressure and suction side.
- NURBS
  - For the SBP model the pointcloud is approximated with NURBS curves [25]. The curves are then approximated as NURBS surfaces and exported as .iges files using the Matlab™ code *nurb2igs.m* [26]. This is a fast way to create the 3D geometry of the blade.
- The XYZ coordinates of the blades have to be exported in .txt format for good control over the geometry in ICEM CFD™.
- The fluid domain is created from a projection of the hub and shroud of the blades to the XZ plane. Along with the inlet of the stator and the outlet of the rotor, this defines the flow path of the flow in a two-dimensional meridional plane. The

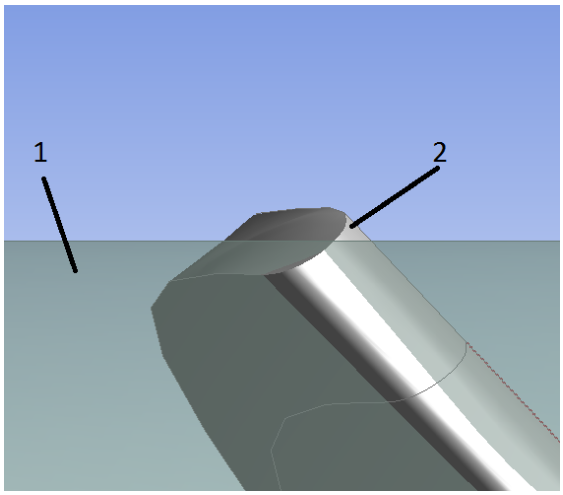

Figure 3.3: Blades need to be extended to account for the tilted blades

XZ coordinates of the flow path are exported from Matlab™ and imported to DesignModeler™ for easier geometry generation.

3.3 Geometry and Mesh

From the performance code the 3D geometry and mesh are generated using two different approaches, one for a single blade passage and another one for the full turbine. Hexahedral mesh is considered rather than a tetrahedral since a hexahedral mesh is more accurate when used appropriately [27]. For the SBP model, DesignModeler™ is used for the geometry and TurboGrid™ is used for the meshing. Regarding the FT model ICEM CFD™ is used both for geometry and meshing. Mechanical™ is used for the structural meshing of the blades.

3.3.1 DesignModeler™

DesignModeler™ is used for the geometry since it provides a good connection between fluid and structural analysis. The surfaces that are exported from Matlab™ are imported to DesignModeler™. As the objective is to have the meshing procedure as automized as possible, an attempt is made to write a script to create the geometry. DesignModeler™ does not support recording of a script for 3D geometry. There is a library with very limited information and guidance for the commands and how to use them. The script imports all the files necessary and then creates the geometry needed for the simulation.

One of the necessary modifications of the performance code is to extend the stator and rotor blades. This is done to create the complete geometry of the blades. The camber lines at the hub and shroud are revolved to form the 3D fluid domain for the turbine. A boolean operation is used to extract the intersection of the fluid domain and the ex-

tended blades resulting in the correct blade height. In Figure 3.4a the extended blades and their intersection with the fluid domain can be seen. In Figure 3.4b the blades have been cut to their real size for all simulations.

Using the DesignModeler™ add-on, BladeEditor, the blades are exported to TurboGrid™. To use the BladeEditor features, two individual flow paths for the stator and rotor are needed. The flow paths are imported with a script directly from the performance code and they define the passage domain as can be seen in Figure 3.4b. The flow path for the stator includes an inlet, hub, shroud and stator outlet. The inlet of the stator corresponds to a small duct between the volute and the stator. The flow path for the rotor inlet shares a boundary with the stator outlet and as for the stator, the hub, shroud and outlet are defined. The rotor outlet is straight and no diffusing is assume for the SBP. The blades and the flow paths are exported to TurboGrid™ with the BladeEditor function *ExportPoints*. After the geometry is imported into TurboGrid™ the flow paths are converted back to 3D.

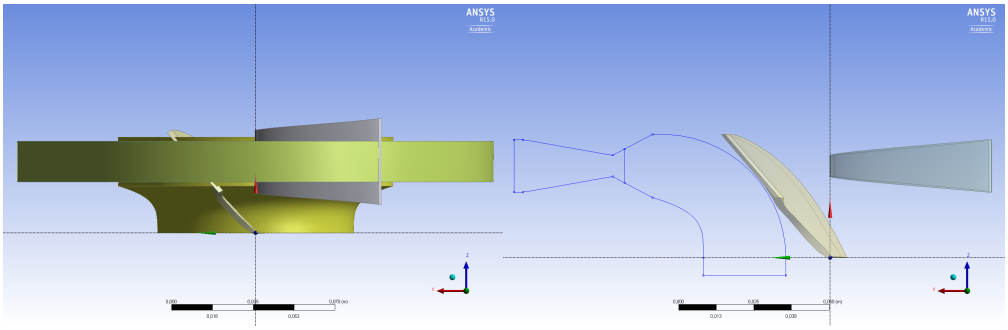

(a) Blades before intersection operation **(b)** Blades after intersection operation

Figure 3.4: Blades before and after the boolean operation

3.3.2 TurboGrid™

TurboGrid™ is used due to its capabilities to highly automate the meshing. The mesh for the rotor and stator is generated individually in TurboGrid™. Using Automated Topology and Meshing (ATM) optimized topology a high quality mesh is generated in a robust way and there is no need for modification of the mesh control points. The average Reynolds number is specified by the script and TurboGrid™ calculates the y^+ value depending on the specific Reynolds number. The method to control the size of the elements in the boundary layer is the *Proportional to mesh size* method. The element size in the boundary layer is controlled by the *Factor Base* and the *Factor Ratio*. To increase the number of elements in the boundary layer the factors are increased [28]. In the SST $k-\omega$ model the transition of the turbulence models is from $k-\omega$ in the inner

region to $k - \varepsilon$ in the outer region and the transition starts at approximately $y^+ = 2$ and ends at approximately $y^+ = 30$.

The shroud tip clearance is specified with the variable normal distance feature in TurboGrid™. The axial and radial clearances are already specified in the Matlab™ code and the gap distance varies linearly in TurboGrid™. An example of the ATM optimized mesh for the stator and rotor for the NASA case can be seen in Figures 3.5a and 3.5b.

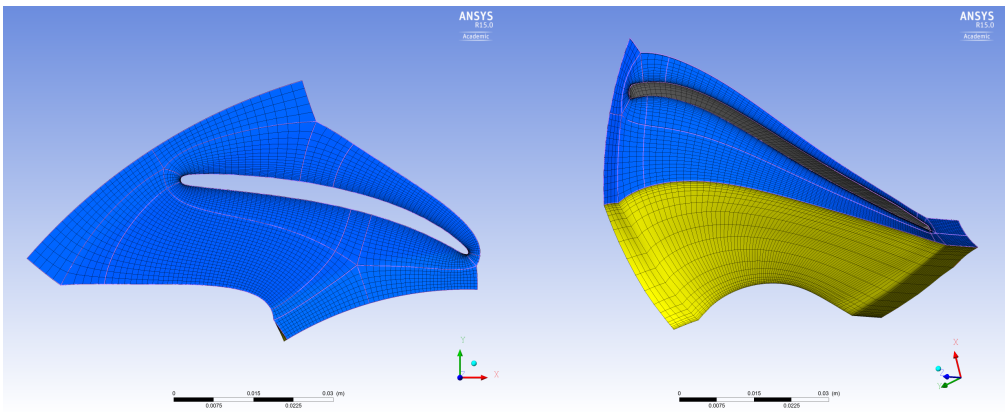

(a) Stator mesh using ATM optimized topology **(b)** Rotor mesh using ATM optimized topology

Figure 3.5: Example of ATM optimized mesh, NASA case

3.3.3 Structural Meshing

For meshing of the structural mesh the Mechanical™ software is used. The software is chosen since it provides good connection between DesignModeler™ and the FEA solver in ANSYS Workbench™.

The meshing tool in ANSYS Workbench™ has been developed to be as automated and user-friendly as possible (Chapter 2.3.2). The mesh for the blades is created with an automatic method which attempts to use sweeping for solid bodies. Simulating swept meshing is much faster as the number elements and nodes are usually much smaller, i.e. larger elements compared to a free mesher. The sweeping tool in ANSYS Meshing™ generates either hexahedral elements or prism elements to follow the geometry as closely as possible. When sweeping is not possible the body is meshed with Patch Conforming Tetrahedron mesher where all faces and boundaries are handled with very small tolerances.

3.3.4 ICEM CFD™

For meshing of the whole turbine the software ICEM CFD™ is used. This software provides a capability to script the process of importing the geometry and meshing the domain. Recording a script is available in ICEM CFD™ and therefore the commands from the graphical user interface can be seen in text command leading to a swift way of finding the right command when scripting the process.

Importing and creating the geometry is complicated in ICEM CFD™ since the main purpose of the software is to mesh existing geometry. The scripting capability and the possibility of generating mesh from complicated geometry outweighs this flaw. One of the main advantages of using ICEM CFD™ compared to TurboGrid™ is that it is able to mesh the volute and the exhaust diffuser. In ICEM CFD™ a high quality mesh can be created with good control over the mesh fulfilling the criteria defined by the CFX™ solver (Chapter 2.2.3). The $y+$ value which is calculated from the Re number is used to specify the wall distance of the near wall elements. This, along with the right turbulence model, ensures that the boundary layers are well resolved. In Appendix B there is a guide to the ICEM CFD™ setup.

3.3.5 Mesh Statistics

In Table 3.2 the mesh statistics for the SBP are given including the number of nodes, elements and the minimum angle for each domain and total.

Table 3.2: SBP mesh statistics

NASA				
Domain	Number of nodes	Number of elements	Minimum angle	Angles $< 20°$ %
Stator	103,500	94,644	61.74	0
Rotor	157,464	145,054	23.11	0
Total	260,964	239,698	-	
ORC				
Domain	Number of nodes	Number of elements	Minimum angle	
Stator	298,908	278,696	20.21	0
Rotor	109,069	99,540	11.06	1.29
Total	407,977	378,236	-	

In Table 3.3 the mesh statistics for the FT are given similar to the SBP previously.
The two tables help to illustrate that much more computational resources are needed

Table 3.3: Full turbine mesh statistics

NASA				
Domain	No. of nodes	No. of elements	Minimum angle	Angles < 20° %
Volute	364,610	347,760	39.96°	0
Stator	361,240	328,548	16.74°	0.3
Rotor	634,464	582,360	20.52°	0
Diffuser	114,221	108,864	12.69°	0.004
Total	1,474,535	1,367,532	-	-
ORC				
Domain	No. of nodes	No. of elements	Minimum angle	Angles < 20° %
Volute	456,192	438,399	36.45°	0
Stator	2,249,752	2,129,520	11.88°	5.670
Rotor	1,556,384	1,467,840	18.81°	1.395
Diffuser	171,992	164,700	16.83°	0.002
Total	4,434,320	4,200,459	-	-

for the FT compared to the SBP model.

3.4 CFX™

The software CFX™ is used to simulate the fluid behavior in the turbine. It offers a specific setup approach for turbomachines to make the set up procedure simpler. Both steady state and transient simulations are performed in CFX™.

Table 3.4: Boundary conditions for CFX™

Properties	NASA	ORC
Fluid	Argon	R143a
Rotational speed	38316 rpm	24492 rpm
Inlet total pressure	0.92559 bar	49.954 bar
Inlet total temperature	1083.3 K	686.1428 K
Outlet static pressure	0.53566 bar	17.992 bar
Inflow vector	[1,0,0]	[1,0,0]

In Table 3.4 the boundary conditions for the CFD simulations are specified. For solving the Navier-Stokes equation, RANS is used for steady simulation and URANS for transient [18]. The turbulence model is the SST $k-\omega$ model due to the good behavior for adverse pressure gradient flows (Chapter 2.2.2). The interfaces between a rotating domain and a stationary domain are modeled as a Stage (Chapter 2.2.4) for the steady case. This includes the interface between stator and rotor as well as the interface between rotor and diffuser. For the transient case the interfaces are modeled as a sliding interface where the transient interaction is resolved between components (Chapter 2.2.4). The disturbances generated upstream of an interface need to be transported downstream. The Rotor Stator disturbance settings are used since it does not require any additional data and that it can be used in both steady and transient simulations (Chapter 2.2.4).

Periodic boundary conditions are needed to simulate the SBP. For the steady simulation the mesh ensures the periodicity. What goes out of one boundary cell goes into the next one on the opposite side. This is called rotational general connection in CFX™. For the transient simulation a more advanced method is needed to ensure the transient behavior of the flow. For the lowest computational time and because of the unequal pitch ratio between components the Time Transformation modeling (Chapter 2.2.4) is used. The Profile Transformation would have required pitch ratio close to unity and the Fourier Transformation needs two blade passages. The FT model is simulated using the same methods as in the SBP model except for the periodic boundary modeling.

In Table 3.5 the number of time-steps for both the SBP and the FT simulation are given. The same timestep is chosen for single blade passage and the whole turbine to keep the simulations of the different methods similar. One period is defined as the time it takes a domain to move the distance of one domain. For the SBP one period is one passage while for the whole turbine one period is one rotation. The timestep has to be chosen small enough for the simulation to be stable and to capture the transient behavior, but still large enough not to waste computational resources. The number of periods has to be large enough for the simulation to reach statistically steady state. The time step is automatically defined by CFX™ from the Courant number and the rotational velocity [18].

Table 3.5: Timestep for transient simulation

	SBP model	FT model
Timestep per period	15	165
Time-step for NASA	$8.69958 \cdot 10^{-6}$s	$8.69958 \cdot 10^{-6}$s
Time-step for ORC	$1.02073 \cdot 10^{-5}$	$1.02073 \cdot 10^{-5}$

3.5 ANSYS Mechanical™

To determine the load and the deflection, a static structural analysis is convenient. Mechanical™ is used to simulate the structural behavior and the sub program Static Structural is used.

One-way fluid structure interaction is used to apply the pressure fluctuations to the blades. The pressure from the solution from CFX™ is imported from the static case to Mechanical. All programs share a single geometry created with DesignModeler™. The boundary conditions on the stator are set as fixed on the hub and shroud but only the hub for the rotor as it has to be able to rotate. Centrifugal forces are dominating over the pressure forces and are included on the rotor blades by adding the rotational speed of the turbine.

The pressure is mapped on the CFD surface. The geometry has to be selected as well as the CFD surface which is transferred from CFX™. Using linear interpolation, mechanical nodal values are calculated from the CFD nodes. The mapping is not always successful but the linear interpolation tolerance can be changed in CFX™. This tolerance controls variable interpolation accuracy on or near boundary surfaces. The value is specified as a percentage of domain extents. To speed up the mapping, a 3D virtual layer of elements is created in the normal direction of the CFD surface and the structural nodes positioned in the surface are mapped. The layer tolerance is either set as a percentage of the domain extent or as a percentage of the average face extent. If the mapping is still unsuccessful and no face is found to map upon, the closest point is chosen.

To determine the deformation of the blade, the total deformation is solved. To have a measure for the stress the von Mises stress (Chapter 2.3.1) is analyzed.

The material chosen for the rotor is a titanium alloy specified in ANSYS Worbench™. The mechanical properties are shown in Table 3.6. This material has good mechanical properties for turbomachinery application; it is light and strong and can withstand the heat requirements. The light material decreases the effect from centrifugal forces.

Table 3.6: Mechanical properties of titanium alloy

Property	Value
Density	$4620 kgm^3$
Young's Modulus	9600MPa
Poisson's Ratio	0.36
Tensile Yield Strength	930MPa
Tensile Ultimate Strength	1070MPa

The time-step and the total time of the simulation in the transient solution have to be specified. The values of the time-step and total simulation time are taken from CFX™. The time-step is calculated in CFX™, but the total time is calculated manually. When the pressure has been imported the time data for the pressure fluctuations can be used to determine the dominating frequencies with an FFT analysis.

3.6 Automized Process

Setting up a CFD simulation from a mean line design code can be time consuming. The geometry has to be created on a specific format from the information obtained by the mean line design and the mesh is then created from the geometry in different software. Making this process as automated as possible by having it macro based can save valuable time and decrease the software experience otherwise needed.

3.6.1 Workbench - Geometry and Mesh

For the SBP model a script will generate the 3D geometry in DesignModeler™. Ideally the script imports the extended blade surfaces and creates a solid body of the blades. The correct geometry of the blades is created with a boolean operation of the intersection of the blades and the revolved hub and shroud camber lines. The flow path of each domain is imported. No information exists on scripting the add-on features of the BladeEditor so they have to be created manually. This is however relatively straightforward and can be carried out quickly compared with previous commands.

The geometry is automatically imported into TurboGrid™. It is recommended to check the mesh quality before continuing to CFX™. When the geometry is complicated, e.g. with a high twist on the blade, TurboGrid™ can fail to create the ATM optimized mesh. Then it is recommended to use an ICEM CFD™ script that has been written and create the mesh in ICEM CFD™. Despite ICEM CFD™ is more robust TurboGrid™ has been preferred as a first option due to the more extensive capabilities in terms of automization.

3.6.2 ICEM CFD™

For ICEM CFD™ a script will create the geometry and set up the mesh. The mesh needs some manual modification to be of a high quality. For some geometries it can be time consuming to create a high quality mesh as it is structured.

3.6.3 CFX™

The simulation setup in CFX™ is done with a script which defines the boundaries, interfaces and all boundary conditions. This makes the process faster since defining the boundaries and boundary conditions require a great deal of different input at various

locations in the software. The only part that needs to be changed manually is the working fluid.

3.7 Definition of Blade Geometry

In Figures 3.6 and 3.7 the definition of the hub, shroud, leading and trailing edges (LE and TE) can be seen. To evaluate the results, three different span locations are chosen, at 5 %, 50 % and 95 % of the span of the stator and rotor blades. The span lines are marked with black in the figures. The blades in the figures are from NASA test case.

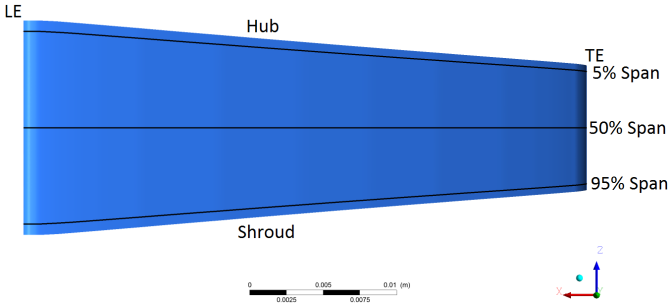

Figure 3.6: Stator blade geometry. Definition of span locations, leading and trailing edge, hub and shroud

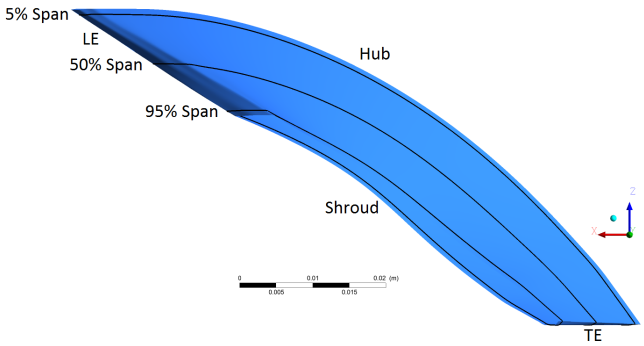

Figure 3.7: Rotor blade geometry. Definition of span locations, leading and trailing edge, hub and shroud

Chapter 4

Results

In this chapter the main results of the project will be presented. The flow of the turbine is studied with the FT model using the NASA and the ORC case. The difference between the SBP and the FT is investigated and the two models compared to the previous studies. The effect of the tip clearance in the SBP is analyzed. The results from the structural analysis are given as a demonstration of what can be done with a titanium alloy as a reference material.

To compare the FT model and the performance code to the SBP models, the performance is evaluated only over the stator and rotor. The stator rotor performance will be addressed as Full Turbine Stator-Rotor and performance code Stator-Rotor.

The results are presented in this chapter and will be discussed in more details in Chapter 5

4.1 Full Turbine

The simulation of the full turbine gives the best result to study the flow. Some interesting phenomena such as a vortex rope appear. It is better to analyze the results of the FT model to draw conclusions from the flow than the SBP as it represents the full turbine geometry. In this chapter the flow result of the components that are not included in SBP will presented.

4.1.1 Volute

The volute distributes the flow and should produce uniform outlet flow. At this stage of the design, the volute could be improved to avoid flow separation.

Separation at entry to stator

In Figure 4.1 a cross section of the volute and the volute stator duct can be seen. At the sharp corners of the volute outlet to the duct the flow separates. The separation extends

to the leading edge and over the stator blades. Entropy generation in other parts of the volute is negligible in comparison.

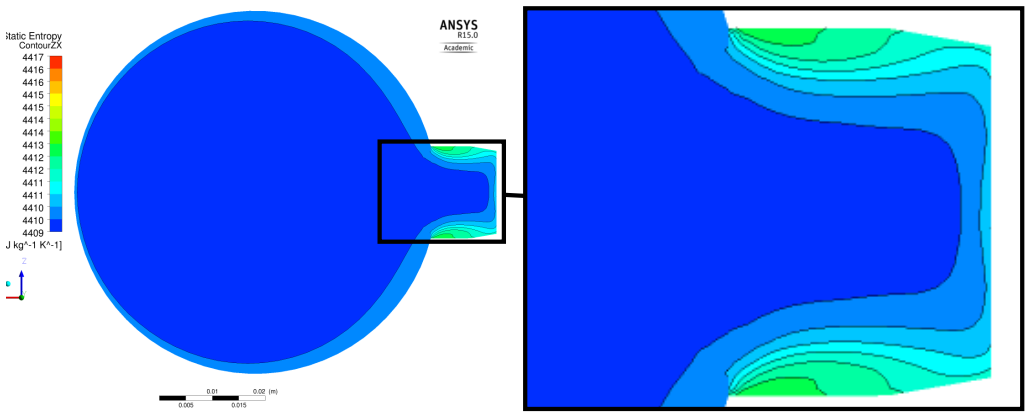

(a) (b)

Figure 4.1: Separation in the volute stator duct, NASA case

Incidence Angle

Figure 4.2b shows a detailed section of Figure 4.2a. The magnified figure shows the first stator blades of the turbine for the NASA case. The streamlines in the figure show how the flow over the first stator blade is affected by the last stator passage. A small separation can be seen on the second blade and a large separation on the third blade. No noticeable or minor separation occurs for the rest of the stator blades.

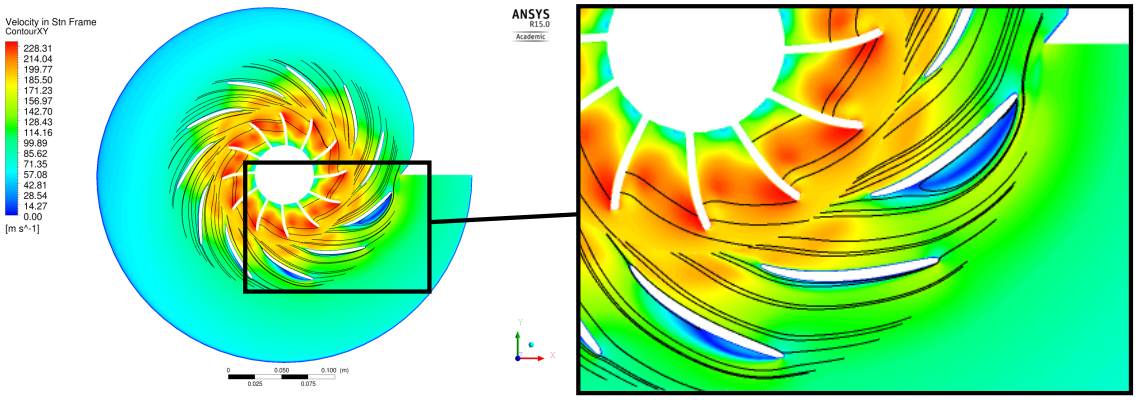

(a) (b)

Figure 4.2: Flow separation over stator blades, NASA case

Comparison of the streamlines for the FT and SBP can be seen in Figure 4.3. In Figure 4.3b it can be seen how the volute gives the correct boundary conditions for the inflow

angle of the stator. In Figure 4.3a the inflow angle has been specified manually and is not ideal. The performance code did not include the inlet to the stator blades so the inlet angle to the stator domain was unknown. This has been addressed in the performance code for future simulations.

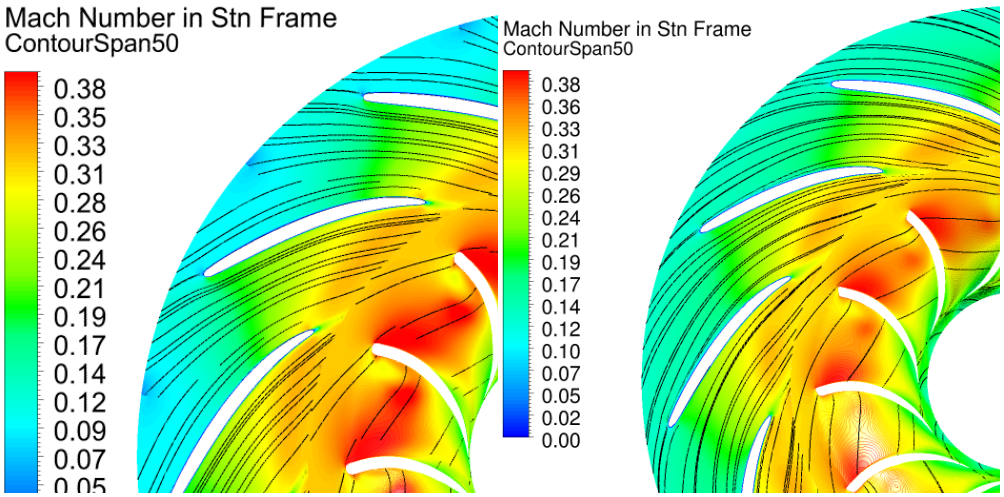

(a) Streamlines in SBP model **(b)** Streamlines in FT model

Figure 4.3: Streamlines for the NASA case

4.1.2 Diffuser

In the diffuser some of the static pressure is recovered through kinetic energy. This is done when the fluid is slowed down, i.e. being diffused.

Vortex Rope

In Figure 4.4 the diffuser for both the NASA and the ORC test cases are shown. Figure 4.4a shows how the outflow for the NASA case is not well distributed over the diffuser outlet and separates at the sphere shaped rotor outlet. For the ORC case this behavior is also noticed in Figure 4.4b but is not of the same magnitude. The outflow for the ORC case is better distributed over the diffuser outlet.

4.2 NASA Test Case

The NASA test case is analyzed by comparing different methods of simulating the turbine. The models are the SBP, SBP with Tip Clearance (SBPTC) and FT model.

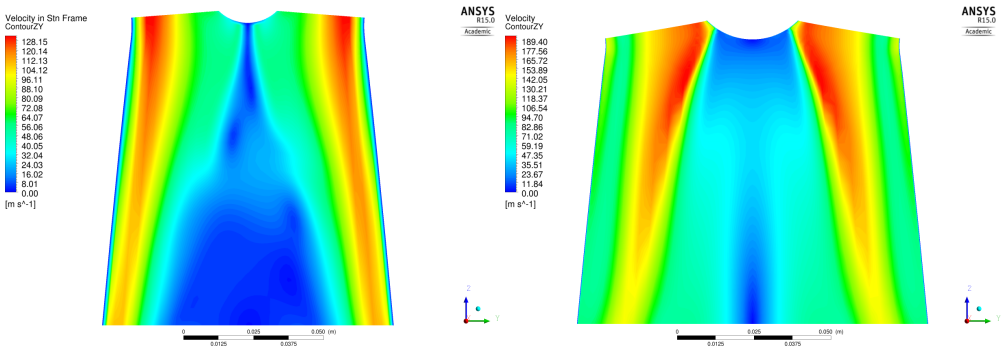

(a) NASA case **(b)** ORC case

Figure 4.4: Velocity contour of the diffuser

4.2.1 Mesh Statistics

Table 4.1 shows the average, maximum and minimum y^+ value for different models for the rotor and stator domains.

Table 4.1: y^+ values for the full turbine and SBP

	y^+ mean	y^+ max	y^+ min
SBP - Rotor	8.9	25.6	0.4
SBP - Stator	26.4	53.1	1.8
Full Turbine - Rotor	38.8	120.0	3.3
Full Turbine - Stator	44.1	85.9	6.7

4.2.2 Performance

In Table 4.2 the total to total efficiency, mass flow and total to total pressure ratio are compared for different simulation methods.

4.2.3 Rotor and Stator Blade Loading

The blade loading for the rotor blade in the SBP is shown in Figure 4.5a at three different span locations (seen in Figures 3.6, 3.7). Figure 4.5b shows the rotor blade loading for the FT, i.e. all 12 rotor blades are included.
The blade loading for the stator blade in the SBP is shown in Figure 4.6a at the three different span locations. Figure 4.6b shows the stator blade loading for the FT, i.e. all 11 stator blades are included.

Table 4.2: Comparison of different models and the NASA test case. This table can not be used to verify the coherence between the performance code and the CFD simulations as discussed in Chapter 5.1

	η_{tt} [%]	Mass Flow [kg/s]	Π_{tt}
Single Blade Passage (SBP)	89.3	0.322	1.70
SBP with tip clearance	87.6	0.319	1.70
Full Turbine Stator-Rotor	88.1	0.315	1.53
Performance code Stator-Rotor	86.3	0.277	1.56
NASA report	88.0	0.277	1.56
Full Turbine	86.6	0.315	1.53
Performance code FT	83.5	0.277	1.59

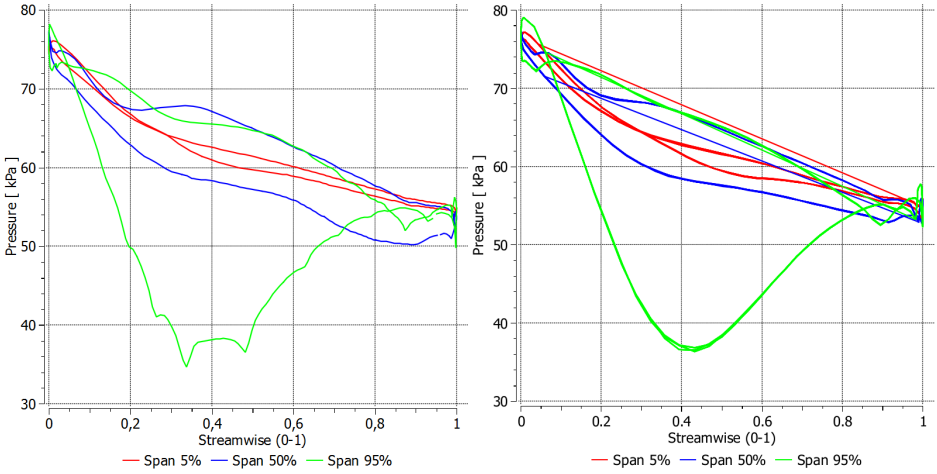

(a) SBP model **(b)** FT model

Figure 4.5: Rotor blade loading at different span locations

4.2.4 Entropy Generation

In Figure 4.7 the entropy generation of the stator and rotor domains can be seen in the meridional view. The entropy is circumferentially averaged. At the stator LE there is more entropy generation for the FT model than for the SBP model. More entropy is generated for whole rotor domain for the FT model compared to the SBP model. A large separation is generated at the hub due to the sharp corner and the diverging intersection from stator to rotor.

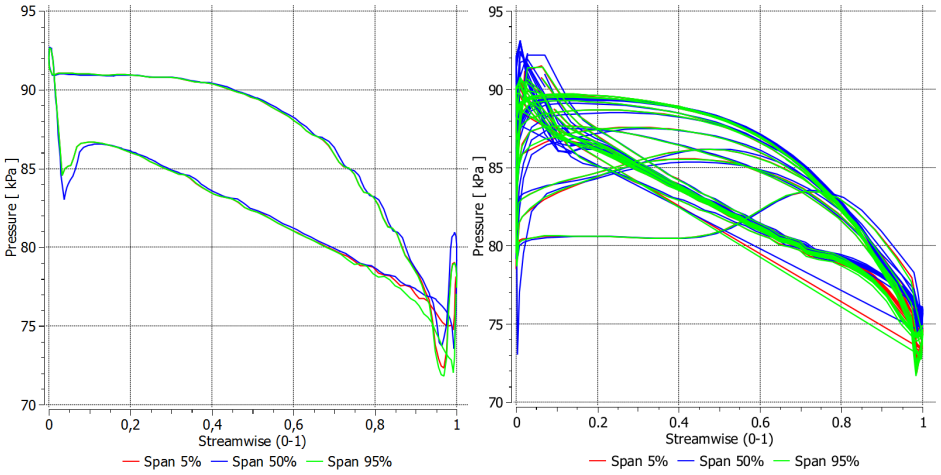

(a) SBP model **(b)** FT model

Figure 4.6: Stator blade loading at different span locations

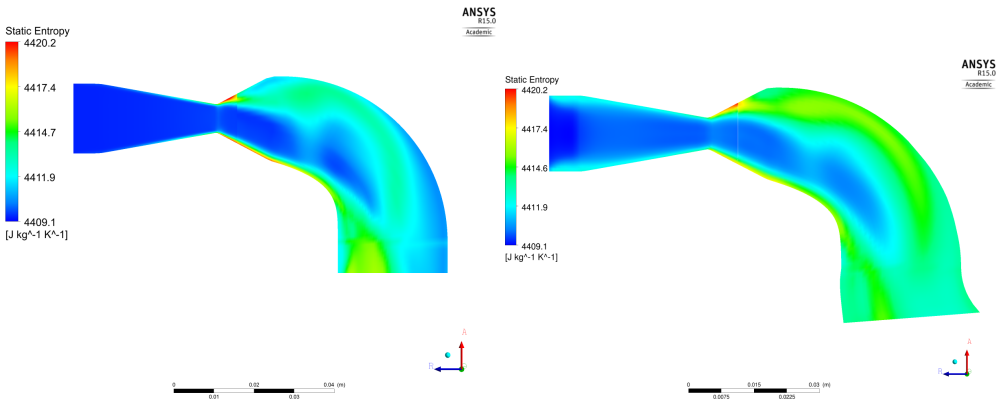

(a) SBP model **(b)** FT model

Figure 4.7: Entropy generation in meridional view NASA case

4.2.5 Structural Analysis

For the structural analysis only the SBP model is considered. The material for structural analysis is for demonstration but gives a realistic result. It shows the capability of the simulation process rather than actual results since the material choice can be very dependent on the turbine.

Stress Analysis

In Figure 4.8 the stress from centrifugal forces and fluid pressure in the rotor blade can be seen. There is a stress concentration at the leading edge hub, seen in the magnified section in Figure 4.8b.

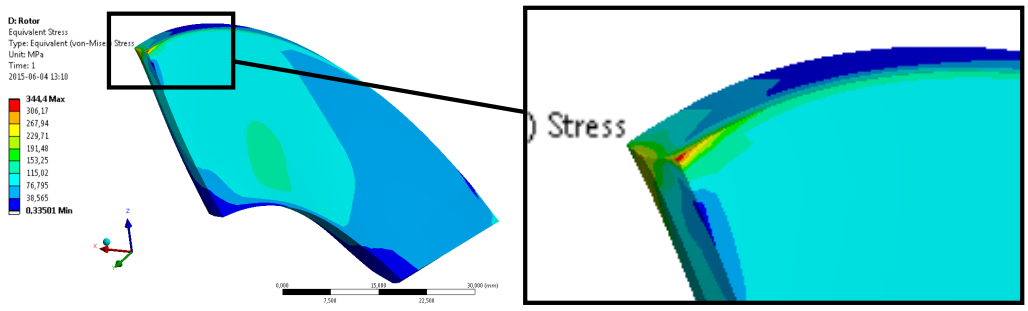

(a) (b)

Figure 4.8: Stresses acting on the rotor blade for the NASA case

4.3 ORC Test Case

The ORC test case is analyzed by comparing different methods of simulating the turbine. This includes the comparison of y^+ values, performance, blade loading and entropy generation.

4.3.1 Mesh Statistics

In Table 4.3 the y^+ mean, minimum and maximum values for different models can be seen for the stator and rotor domains.

Table 4.3: y^+ values for the FT and SBP

	y^+ mean	y^+ max	y^+ min
SBP - Rotor	26.6	70.1	0.5
SBP - Stator	67.1	131.6	1.4
Full Turbine - Rotor	293.0	767.6	6.2
Full Turbine - Stator	199.4	562.8	7.5

4.3.2 Performance

In Table 4.4 the performance of the turbine for different methods is shown. There the total to total efficiency, mass flow and total to total pressure ratio are compared. The results in the lower half of the table are calculated from the stator inlet to the diffuser outlet.

4.3.3 Rotor and Stator Blade Loading

The blade loading for the rotor blade for the SBP is shown in Figure 4.9a at three different span locations. Figure 4.9b shows the rotor blade loading of the FT, i.e. all rotor

Table 4.4: Comparison of different models and the ORC test case. This table can not be used to verify the coherence between the performance code and the CFD simulations as discussed in Chapter 5.1

	η_{tt} [%]	Mass Flow [kg/s]	Π_{tt}
SBP	79.2	21.4	2.30
SBPTC	79.3	21.4	2.30
Full Turbine Stator-Rotor	75.4	20.8	2.10
Performance code Stator-Rotor	89.0	17.2	2.59
Full Turbine	75.4	20.8	2.40
Performance code	88.0	17.2	2.62
ORC report	79.8	17.2	2.62

.

blades are included.

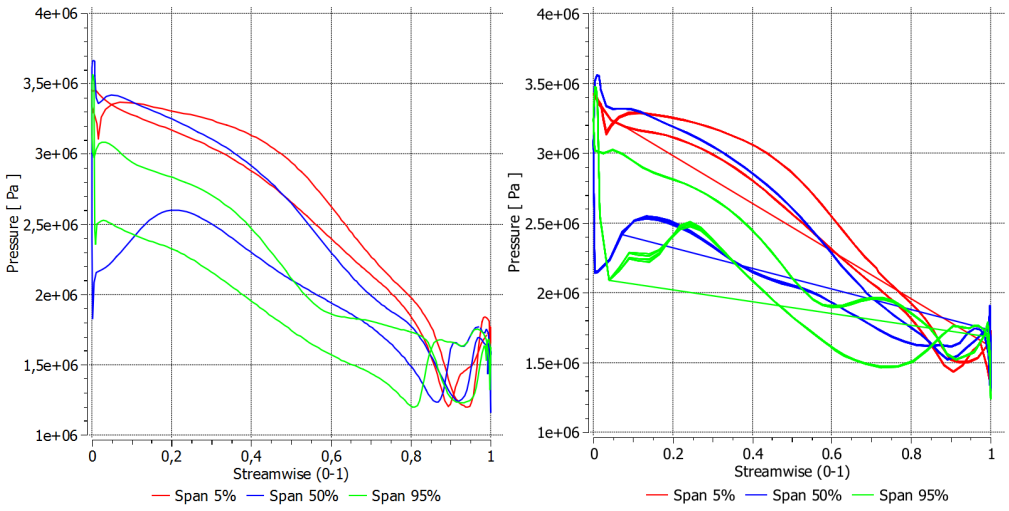

(a) SBP model **(b)** FT model

Figure 4.9: Rotor blade loading at different span locations

The blade loading for the stator blade of an SBP is shown in Figure 4.10a at three different span locations. The Figure 4.10b shows the stator blades blade loading of the full turbine, i.e. all stator blades are included.

4.3.4 Entropy Generation

In Figure 4.11 the circumferentially averaged entropy generation is shown for both the SBP and the FT simulation in the meridional view. In Figure 4.11a it can be seen how

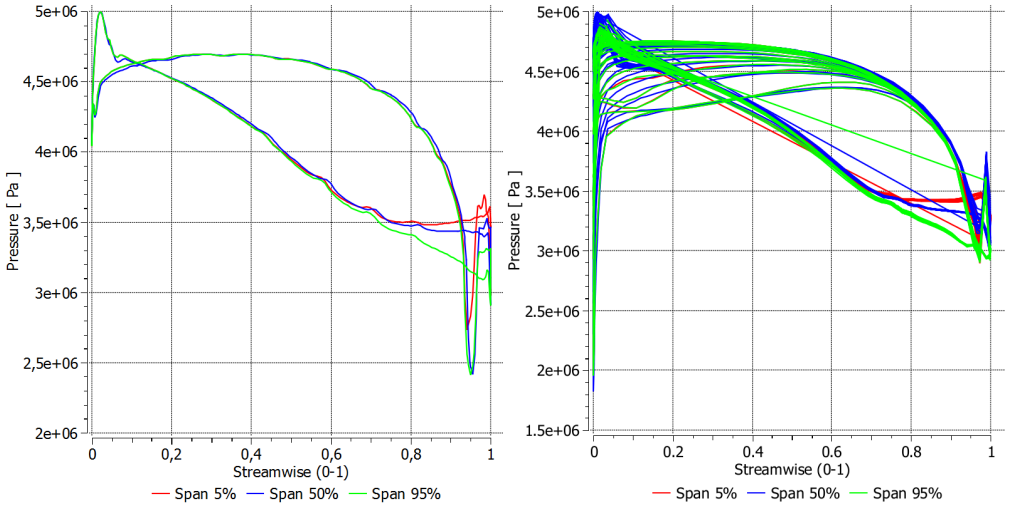

(a) SBP model **(b)** FT model

Figure 4.10: Stator blade loading at different span locations

the entropy generation is negligible in the stator domain but a large entropy generation at the rotor TE shroud. There is also a small peak at the TE hub. Figure 4.11b shows the entropy generation for the FT model. For the stator domain, entropy is generated at the hub and shroud. In the duct between the stator and rotor for the full turbine case, there is a small peak at the shroud. For the rotor domain, the entropy generation is large at the TE hub but there is no peak at the TE shroud as for the SBP. A separation can be seen in the stator rotor intersection due to the sharp corner at the stator trailing edge and the diverging intersection from stator to rotor. Large entropy generation can be seen at the rotor shroud outlet.

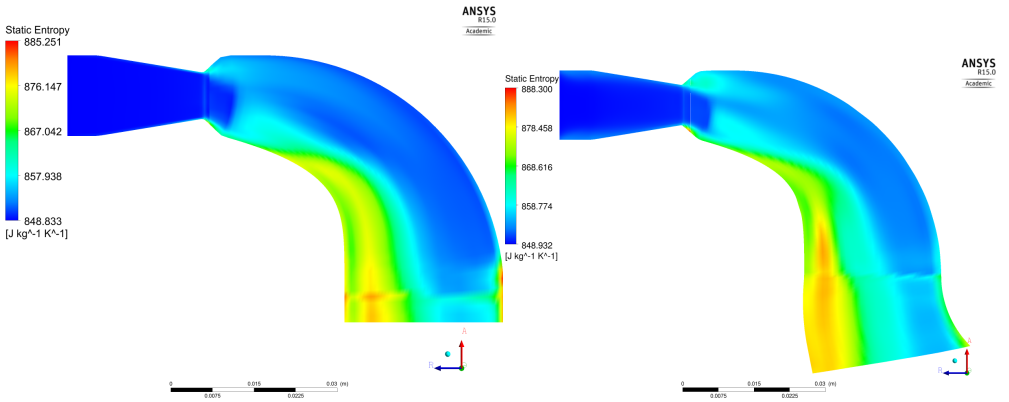

(a) SBP model **(b)** FT model

Figure 4.11: Entropy generation in the meridional view for ORC case

4.3.5 Partly Choked Passage

The rotor blade passage is partly choked, i.e. the Mach number is equal (or greater) than 1 in part of the passage. In Figure 4.12 the rotor blade passage can be seen at 50% span where the passage is choked. The passage is only partly choked since the Mach number is less than one at some span locations.

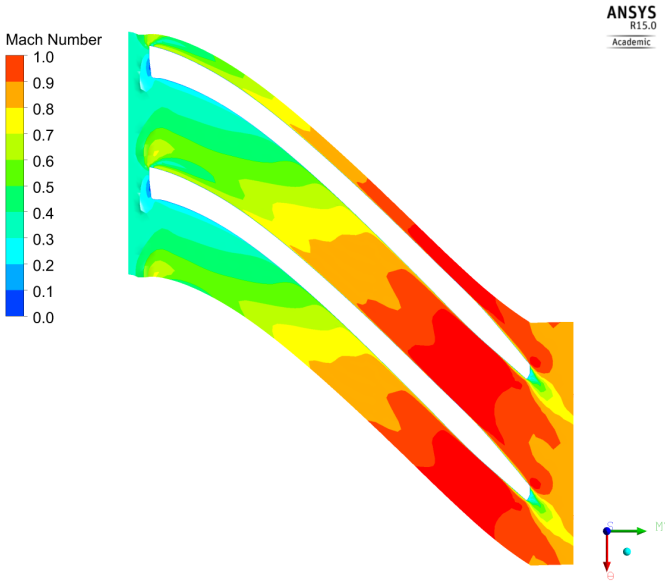

Figure 4.12: The rotor blade passage at 50% span is choked

4.3.6 Structural Analysis

For the structural analysis only the SBP model is considered. The material for structural analysis is for demonstration but gives a realistic result. It shows the capability of the simulation process rather than actual results since the material choice can be very dependent on the turbine.

Stress Analysis

In Figure 4.13 the stress from centrifugal forces and fluid pressure in the rotor blade can be seen. There is a stress concentration at the leading edge and mid blade hub seen in the magnified section in Figure 4.13b.

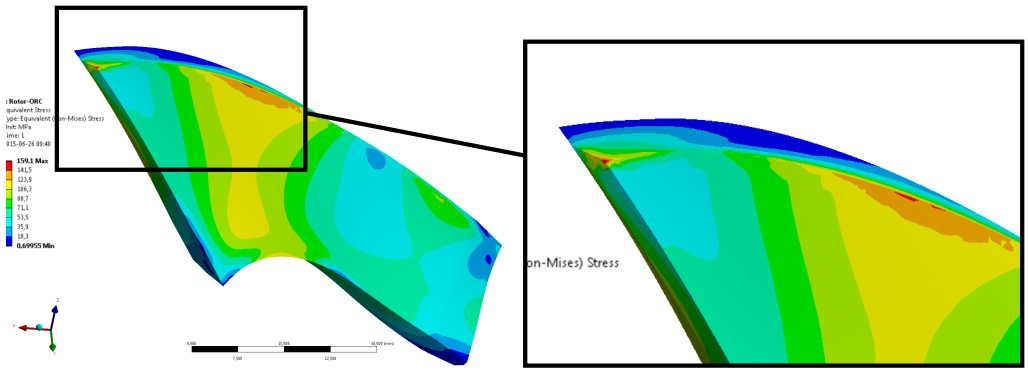

(a) (b)

Figure 4.13: Stresses acting on the rotor blade for the ORC case

Chapter 5

Discussion

In this chapter the result will be analyzed and discussed in further detail.

5.1 Simplifications to Model

The CFD simulations carried out in this thesis have given valuable feedback to the performance code resulting in different assumptions being modified like discussed in Chapter 3.2. The CFD simulations are carried out with these modifications so they can not be compared directly to the original performance code. The performance code is designed in such a way that it does not affect the performance of the turbine, where the performance is the input while the geometry is the output which is used in the CFD simulations. The results from the 3D CFD simulations are then highly dependent on the geometry given from the performance code. This effect can clearly be seen in Tables 4.2 and 4.4.

An ongoing development of the performance code by changing the stator rotor intersection is being carried out and gives a promising preliminary result decreasing separation in the intersection. The separation at the stator TE is considered as it seems to be rather high. Instead of the constant absolute velocity assumption which gives the diverging intersection a constant cross section between the stator and rotor blades is assumed.

5.2 Full Turbine

In Figure 4.1 the separation due to the circular cross sectional design at the volute outlet can be seen. The separation extends to the stator blades increasing losses in the turbine. The separation is caused by the sharp edge between the volute outlet and the duct between the volute and stator and is directly related to the volute design. The outlet of the volute has not been optimized in the performance code with respect to the geometry. It has been designed to deliver the flow properties uniformly to the stator rows. By considering a design shown in Figures 3.1b and 3.1c the separation in the volute outlet can be decreased. The asymmetric design in Figure 3.1b is expected to decrease the separation and should be relatively easy to implement in the performance

code. The trapezoidal cross section in Figure 3.1c is harder to describe algebraically but will probably have the smallest separation of those three shapes.

Figure 4.2 shows the streamlines in the XY plane. Due to a sharp end in the volute, too much flow is directed to the last passage, and the flow is forced to the first passage. This partly due to the simplification made in the volute end 3.2. This results in large separation at the first stator. At the second and third stator blades the separation is created by the incidence angle as described in Figure 2.3. The position of the stator row can be aligned to the volute end in order to minimize the separation. If there is still large separation, the first stator blade can be extended to the volute to have a closed volute. As a result the incidence on the first blades would be closer to zero as the flow distribution would be more even.

The boundary condition of the volute inlet is defined as a velocity normal to boundary. As can be seen in Figure 4.2, the inlet is not uniform since it seems that the flow from the volute end is affecting the inlet. This causes the flow to be non-uniform at the stator inlet for the first four blades making the incidence angle deviate from the ideal incidence. For the rest of the stator blades the separation is negligible underlining the effects from the inlet. To decrease the separation the inlet condition could be defined with an angle to the boundary directing the flow to the stator rows.

The streamlines in Figure 4.3 show the direction of the inlet velocity for the SBP and the FT. The inflow direction is specified manually for the SBP seen in Figure 4.3a. For the best performance the stator incidence should be close to zero. This can be hard to obtain without running the simulation and measuring the incidence. For the best incidence angle it has to be iterated for the SBP model. The stator inflow angle is defined in the performance code at the leading edge of the blade. To extend the angle to the inlet of the stator blade domain a rough estimation is used. In future simulations this has been addressed in the performance code and the stator domain inlet angle should be specified. For the FT the volute distributes the flow evenly to the stator blades making the incidence dependent on the volute design. Comparing the streamlines in Figures 4.3a and 4.3b the inflow has close to zero incidence for the FT while for the SBP the inflow has a negative incidence, i.e. impacting the blades from above.

A vortex rope [29] is generated in the diffuser for both cases, as can be seen in Figure 4.4. This should not have a great impact on the efficiency. The vortex rope can create pressure fluctuations which can damage the turbine if the frequencies match one of the turbine eigenfrequencies. Comparing the two cases, the NASA case seems to have larger stagnation area than the ORC case. This could be because the highest diffuser inlet velocity for the ORC case is at a smaller distance from the rotational axis, increasing the velocity closer to the center.

5.3 NASA Test Case

The y^+ value is important for the turbulence model. As was discussed in Chapter 2.2.3 the y^+ should be in the range of 30-300. By comparing the values in Table 4.1 it can be seen that the y^+ value is well under the higher bound. The SBP simulation is faster and therefore the boundary layer can be resolved giving y^+ values below 30. The SST $k-\omega$ uses automatic wall function (Chapter 2.2.4) so the near wall elements can be refined more than $y^+ = 30$. Since it is not in the scope of this project to investigate the mesh dependency no further investigation was carried out. To ensure that the y^+ value falls within the limit, it has to be checked after the simulation as the true Reynolds number is not known before the simulation (2.2.3).

The total to total efficiency, mass flow and total to total pressure ratio for the SBP, both with and without tip clearance, the FT simulations, the performance code and the NASA report are compared in Table 4.2. Both SBP cases have higher efficiency than the performance code. The SBP without tip clearance has higher efficiency than the NASA case while the SBP with tip clearance has lower efficiency. This is to be expected since the tip clearance leakage is working fluid that does not contribute as useful work. To compare the FT model to the NASA case, the efficiency is evaluated over the stator and rotor blades, using the volute and diffuser only as boundary conditions. The FT Stator-Rotor model has similar efficiency as the NASA case and the SBP models, but slightly higher than the performance code. What comes as a surprise is that the mass flow is higher than the performance code and the NASA report for all CFD models. This could be because the blockage model for the performance code over predicts the blockage in the turbine decreasing the mass flow for the blade design. This would result in higher mass flow for the CFD simulations both for the CFD models. The total to total pressure ratio is highest for both SBP cases but the FT and the full turbine performance code have the same pressure ratio. The higher pressure ratio for the SBP could be investigated further with a mesh dependent study. The boundary conditions, both inlet and outlet, could influence the pressure ratio over the turbine. The inlet boundary conditions for the SBP are circumferentially averaged from the performance code and the outlet boundary conditions are averaged over the rotor outlet. The outlet of the rotor domain in the SBP is simplified and does not take the diffuser into account. This might cause the boundary conditions to vary from the correct value giving incorrect pressure ratio.

The rotor blade loading is compared for SBP and FT in Figure 4.5. The FT rotor blade loading is for all the blades. Since the inlet to the rotor domain is circumferentially averaged all the rotor blades have the same inlet condition and are supposed to have the same blade loading (Chapter 2.2.4). If there is a difference between blades, it is due to the convergence criteria. If the convergence criteria were stricter, the difference should decrease. The blade loading has similar behavior for both the SBP and the FT. At the 5% and 50% span the results are almost identical. There is a fluctuation at the 95% span for the SBP between 0.35 to 0.55 in the streamwise direction which might be

because of the convergence criteria and the mesh resolution. From the figures it can be seen that the further away from the hub the more energy is extracted from the flow.

The stator blade loading in Figure 4.6 shows a comparison between the SBP and the FT. For the FT model each stator has different loading since there is no averaging between the volute and the stator. This gives an approximation closer to the true flow through the stator. There are 5 blades that differ from the main trend and the SBP behavior, the last blade and the first four. As discussed previously the first four blades are influenced by the volute end. A part of the flow cannot enter the last blade passage and is diverted to the first passage causing the incidence angle to deviate significantly from zero. The last blade is affected from the volute end. Due to the increased mass flow through the last passage, the blade loading differs from the SBP. The volute is designed to distribute the flow evenly to each blade passage by decreasing the cross sectional area. The simplifications in the volute end (Chapter 3.2) change the designed area resulting in increased mass flow to the last blade passage.

The blade loading at the LE and TE are different for the FT compared to the SBP. That is because of the different instantaneous incidence angle in the FT. The loading is a little fluctuating for the stator in the SBP which indicates, as for the rotor, that the convergence could be stricter and the mesh refined. The blade loading at both 5% and 95% span is symmetric around the 50% span except for the TE region where the rotor starts to break up the symmetry. This is the case for both the SBP and the FT.

The entropy generation is useful when trying to identify where the losses take place and in what magnitude. Figure 4.7 compares the SBP and the FT entropy magnitude in meridional view. The FT has lower efficiency (Table 4.2) and thus more entropy generation is expected. The larger entropy generation in the stator of FT model is because of the influence from the sharp outlet corner of the volute which increases separation. For the rotor domain the entropy magnitude is considerably larger for the FT than for the SBP. From the figure it can be seen that the stator domain outlet influences the entropy magnitude in the rotor. Therefore the entropy magnitude is larger for the rotor domain in the FT simulation. The reason for the higher entropy magnitude at the hub is a separation at the LE hub due to the downward direction of the flowpath. This large separation is transformed downstream creating large highly turbulent region in the domain.

The von Mises stress for the rotor blade in the SBP simulation is shown in Figure 4.8. The maximum centrifugal stress occurs at the blade root where the blade is fixed to the hub. The peak at the LE hub is probably because there is a sharp edge and the hub has a fixed boundary condition. If the rotor hub was included, i.e. the part that the blades are fastened to and a fillet between, the stress distributions would be more realistic to a final design of a turbine and this peak would not exist. Even though this is the case, the highest stress value is still well below the yield limit, which can be seen

in Table 3.6, with a safety factor of 2.7. Considering the blade loading on the rotor in Figure 4.5 and comparing it with Figure 4.8 it shows that the centrifugal forces are dominant. The pressure from the fluid has a maximum value of approximately 0.8 MPa compared to approximately 340 MPa from centrifugal forces.

5.4 ORC Test Case

The y^+ value is important for the turbulence model. With reference to what is discussed in Chapter 2.2.3 the y^+ should be in the range of 30-300. By comparing the values in Table 4.3 it can be seen that the y^+ value is well under the higher bound for all values of the SBP but only for the mean and minimum value for the FT. Since it is not in the scope of this project to investigate the mesh dependency no further study was made. To ensure that the y^+ value falls within the limit, it has to be checked after the simulation as the true Reynolds number is not known before the simulation (Chapter 2.2.3). The reason for the large y^+ value is because the model is computationally demanding and modifications of the mesh were not considered after the simulation. The SBP simulation is faster and therefore the boundary layer can be resolved giving y^+ values below 30. Since the SST $k-\omega$ uses automatic wall function (Chapter 2.2.4), the near wall elements can be refined more than $y^+ = 30$.

The total to total efficiency, mass flow and total to total pressure ratio for the SBP, both with and without tip clearance, the FT simulations, the performance code and the ORC report are compared in Table 4.4. The efficiency for the SBP is lower than the performance code but similar to the ORC report. The FT simulation has the lowest efficiency of all. The performance code efficiency is much higher than both the CFD and the ORC report; that is because of under estimation of losses in the performance code or insufficient mesh density in the CFD simulation and should be investigated further. The mass flow from the CFD simulations is larger than for both the performance code and the ORC report but the blockage model could be the reason for the higher mass flow as was mentioned in relation to the NASA case. The total to total pressure ratio is lowest for both SBP cases. For the FT the pressure ratio is closer to the report but still lower than the performance code and the ORC report.

The rotor blade loading is compared for SBP and FT in Figure 4.9. The FT rotor blade loading is for all the blades. Since the inlet to the rotor domain is circumferentially averaged all the rotor blades have the same inlet condition and are supposed to have the same blade loading (Chapter 2.2.4). If there is a difference between blades it is due to the convergence criteria. If the convergence criteria were stricter, the difference should decrease. The blade loading has similar behavior at 5% and 50% span in the SBP and the FT while there is more difference at the 95% span, especially at the LE. Most of the energy is extracted from the blades at the 50% span, compared to at 95% for the NASA case. The TE is quite different for all span locations and there the diffuser could be important.

The stator blade loading in Figure 4.10 shows the comparison between the SBP and the FT. For the FT each stator has different loading since there is no averaging between the volute and the stator. This gives the true flow through the stator. There is only one stator blade that differs much from the others for the FT simulation, the first blade from the volute inlet. The other stator blades still have slightly different blade loading but follow the main trend. This shows that the ORC volute performs better than the NASA volute and how the design can have an impact on the flowfield. The blade loading at the LE and TE are different for the FT compared to the SBP. That is because of the different incidence angle in the FT. The loading is a little fluctuating for the SBP for the stator blades which indicates, as for the rotor, that the convergence could be stricter and the mesh refined. The blade loading at 5% and 95% span is symmetric around the 50% span, except for the TE region where the rotor starts to break up the symmetry. This is the case for both the SBP and the FT.

Similar to the NASA case entropy generation is useful to identify where the losses take place and in what magnitude. Figure 4.11 compares the SBP and the FT entropy in meridional view. The FT has lower efficiency (Table 4.4) and more entropy generation is expected. The larger entropy magnitude in the stator of FT model is because of the influence from the sharp outlet corner of the volute that increases separation. This is not as large a factor as for the NASA case and could be because of higher velocities. For the rotor domain the entropy magnitude is considerably larger for the FT than for the SBP. From the figure it can be seen that the stator domain outlet influences the entropy magnitude in the rotor. Therefore the entropy magnitude is larger for the rotor domain in the FT simulation. The reason for the higher entropy magnitude at the shroud is that the high velocities partly choke the rotor passage.

The rotor blade passage is partly choked, as seen in Figure 4.12. The Mach number is greater or equal to 1 across the entire passage at specific span locations but not all. Choked passage means the mass flow rate cannot increase with decreased downstream pressure. The partly choked passage will limit the mass flow rate in the choked areas but increase the flow in non-choked areas. This could increase losses in the turbine especially due to the increased mass flow where the passage is not choked.

The von Mises stress for the rotor blade in the SBP simulation is shown in Figure 4.13. The peak at the LE and mid blade hub is probably because there is a sharp edge and the hub has a fixed boundary condition. If the rotor hub was included, i.e. the part that the blades are fastened to and a fillet between, the stress distribution would be more realistic and this peak would not exist. Even though this is the case, the highest stress value is well below the yield limit, which can be seen in Table 3.6, with a safety factor of 5.8. Considering the blade loading on the rotor in Figure 4.9 and comparing it with Figure 4.13 it shows that the centrifugal forces are dominant. The pressure from the fluid is at maximum approximately 3.5 MPa while the maximum stress from the

centrifugal forces is approximately 159 MPa.

Chapter 6

Conclusion

The objective of the thesis was automate the process of setting up a CFD simulations. It can be concluded from the thesis work that the process can be simplified to a large extent. The performance code has been further developed and a script written that reduces the amount of time needed to set up the geometry and mesh. For the FT model, setting up the geometry and the blocks for the mesh was very time consuming but is now fully automatic using a script in ICEM CFD™. To create a high quality mesh some modifications and experience in the software is most likely needed. The same applies to the SBP method: creating the geometry has been made much easier with a macro based script in DesignModeler™. The methods developed for the FT and the SBP have shown good results for most geometries. When the geometry is more complex, e.g. more twist on the blades, some manual modifications might be necessary. The process can possibly be further developed with more knowledge and experience in java scripting in DesignModeler™ for the SBP. The set up time is also highly dependent on mesh density that depends on flow velocity.

Comparing the SBP and the FT model it can be concluded that the SBP can provide a good estimate of the performance, e.g. efficiency and blade loading. To ensure the quality of the 3D geometry the FT model has to be used to simulate the volute and as well as the diffuser. It can be concluded that the performance code is a promising tool but could be improved further to generate even more accurate representation of radial turbine that could finally be manufactured. The future developments involve better geometrical representation, including the volute inlet and outlet, trailing edge of the stator and leading edge of the rotor. From the CFD results it can be concluded that the performance code sometimes overpredicts the efficiency and could give a better estimate if the passage is partly choked in the rotor channel.

6.1 Future Work

There are some features that can be improved in future work. For the geometrical design the volute needs the most improvements. As mentioned before, the volute design is not

optimized geometrically. This can be improved and separation possibly avoided. The inlet duct of the volute could be included for a more detailed representation of the radial turbine.

The 3D representation of the blades is calculated from the camber lines. The camber lines should define the maximum radius of the rotor leading edge. This is not the case in the performance code as it is today but is a work in progress.

The SBP model has one feature that the FT model is missing and that is the tip clearance. Including the tip clearance in the FT model would be a M.Sc. thesis in itself. It would be interesting to see the results from such a model compared to the current one.

A method to generate the mesh and to make the whole process completely automatic is of great interest. Using ANSYS Workbench to create a tetrahedral mesh for the fluid domain should allow the process to be more adaptive to different geometries.

An ongoing development of the performance code by changing the stator rotor intersection is being carried out and gives a promising preliminary result. The separation at the stator TE was considered as it seemed to be rather high. This was done by assuming constant cross section between the stator and rotor blades instead of the constant absolute velocity assumption, which gave the diverging intersection. The entry before the stator, the trailing edge thickness of the stator and rounding of the rotor leading and trailing edges has been addressed in the performance code and should be available in future studies.

6.2 Contribution

The thesis work was carried out in close cooperation of both students. However it could be said that Elias Siggeirsson was mainly responsible for the FT model while Steinn Gunnarsson was mainly responsible for the Single Blade Passage model; both were though much involved in both models. The writing of the thesis was evenly divided with ongoing discussions about the project as a whole.

Bibliography

[1] T. N. I. of Standards, T. (NIST), Refprop user's guide (2007).
URL http://www.nist.gov/srd/upload/REFPROP8_manua3.htm#appendixa

[2] J. Mowill, L. Axelsson, Axial and radial turbines (2015).
URL http://www.kinsley-group.com/files/documents/Axial%20and%20Radial%20Turbines_TMI%2011-12_p%2032.pdf

[3] S. Dixon, C. Hall, Fluid Mechanics and Thermodynamics of Turbomachinery, 7th Edition, Elsevier Inc., Wyman Street, Waltham, USA, 2014.

[4] H. Moustaphe, M. Zelesky, N. Baines, D. Japikse, Axial and Radial Turbines, Concepts NREC, White River Junction, Vermot, 2003.

[5] Y. Çengel, M. Boles, Thermodynamics: An engineering approach, 2nd Edition, NY: McGraw-Hill, New York, 1994.

[6] O. Balje, Turbomachines - A guide to design, selection and theory, 1st Edition, Wiley, New York, 1981.

[7] S. Yahya, Turbines Compressors and Fans, Tata McGraw-Hill Education Pvt Ltd., New Delhi, 2011.

[8] E. J. Logan, R. Roy, Handbook of Turbomachinery, 2nd Edition, M. Dekker, New York, 2003.

[9] H. G. F., J. I. H., Experiments concerning the aerodynamic performance in inward radial flow turbines, Proc. Inst. Mech. Eng. 178 (1963) 28–42.

[10] G. Sovran, Fluid mechanics of internal flow, 1st Edition, Elsevier, New York, 1967.

[11] F. Menter, Improved two-equation $k-\omega$ turbulence models for aerodynamic flows.

[12] H. Versteeg, W. Malalasekera, An Introduction to Computational Fluid Dynamics, 2nd Edition, Pearson Education Limited, Edinburgh Gate, Harlow, 2007.

[13] F. Menter, Two-equation eddy-viscosity turbulence model for engineering applications, AIAA Journal 32 (1994) 1598–1605.

[14] D. Wilcox, Reassassment of the scale-determening equation, AIAA Journal 26 (1988) 1299–1310.

[15] ANSYS, ANSYS CFX-Solver Modeling Guide, 275 Technology Drive, Canonsburg, PA 15317, 15th Edition (2013).

[16] F. White, Viscous Fluid Flows, 2nd Edition, McGraw-Hill, New York, 1991.

[17] M. Giles, Calculation of unsteady wake/rotor interaction, Propulsion 4 (1988) 356–362.

[18] ANSYS, ANSYS CFX-Solver Theory Guide, 275 Technology Drive, Canonsburg, PA 15317, 15th Edition (2013).

[19] R. Budynas, Shigley's mechanical engineering design, Mcgraw Hill Higher Educat, S.l, 2009.

[20] O. U. Press, Oxford dictionaries (2015).
URL `http://www.oxforddictionaries.com`

[21] M. Kofikey, D. Holeski, Cold performance evaluation of a 6.02 inch radial inflow turbine designed for a 10-kilowatt shaft output brayton cycle space power generation system, Tech. rep., National Aeronautics and space administration (1966).

[22] E. Sauret, Y. Gu, Three-dimensional off-design numerical analysis of an organic rankine cycle radial-inflow turbine, Applied Energy 135 (2014) 202–211.

[23] CFturbo, Volute cross section (2015).
URL `https://en.cfturbo.com/fileadmin/content/manual/en/cross_section.html`

[24] R. Aungier, Turbine Aerodynamics, ASME, New York, 2006.

[25] L. Piegl, W. Tiller, The NURBS Book, 2nd Edition, University of Computer Science and Engineering, Tampa, Florida, 1997.

[26] MathWorks, Nurbs2iges (2015).
URL `http://www.mathworks.com/matlabcentral/fileexchange/12087-nurbs2iges`

[27] Ansys, Turbocharger design & analysis solutions (2012).
URL `http://www.ansys.com/staticassets/ANSYS/staticassets/resourcelibrary/presentation/auto_conference_turbochargers_2012_Holmes_Hutchinson1.pdf`

[28] ANSYS, ANSYS TurboGrid User's Guide, 275 Technology Drive, Canonsburg, PA 15317, 15th Edition (2013).

[29] H. Foroutan, Simulation, analysis and prevention of vortex rope in hydraulic turbine draft tubes (2015).
URL `http://sites.psu.edu/foroutan/research/`

Appendix A

Appendix 1 - SBP Guide

A.1 DesignModeler™

ANSYS Workbench 15.0 is used for the SBP. To create the geometry a script is run in ANSYS Workbench™. The script creates a new Geometry component and runs the a javascript to generate the geometry and the flow path. The add on *BladeEditor* feature is used to export the geometry to TurboGrid™. There is no information of scripting the features of the *BladeEditor* add on, and the features have to be created manually. As it is today, the script works for all geometries, but there has been some problems previously which might come up again.

To create the geometry:

- Open ANSYS Workbench 15.0
- Run the script file
  - Select *File* > *Scripting* > *Run script file...* and open *WorkbenchScriptDesignModeler_out.wbjn* which should be in the *RunScripts* folder

The script opens DesignModeler™ and generates the geometry similar to Figure A.1. If the surface marked with 1 and the lines marked with 2 in Figure A.1 are not visible, make sure that the units are correct in DesignModeler™. In the same bar as *File*, open *units* and make sure that the unit checked is *m*.

In Linux: The decimal separator is a period, opposed to a comma in Windows. The script assumes Windows operating system, so if the script is run in Linux, an error is expected which can be seen in Figure A.2. Do not accept the correction, but make sure that the Body Operation *BodyOp1* is successful. By declining the correction the *User Tolerance* is set to 0.0015 which should be fine, but can be decreased to 0.0001 by clicking the value, change it and generate using the F5 button.

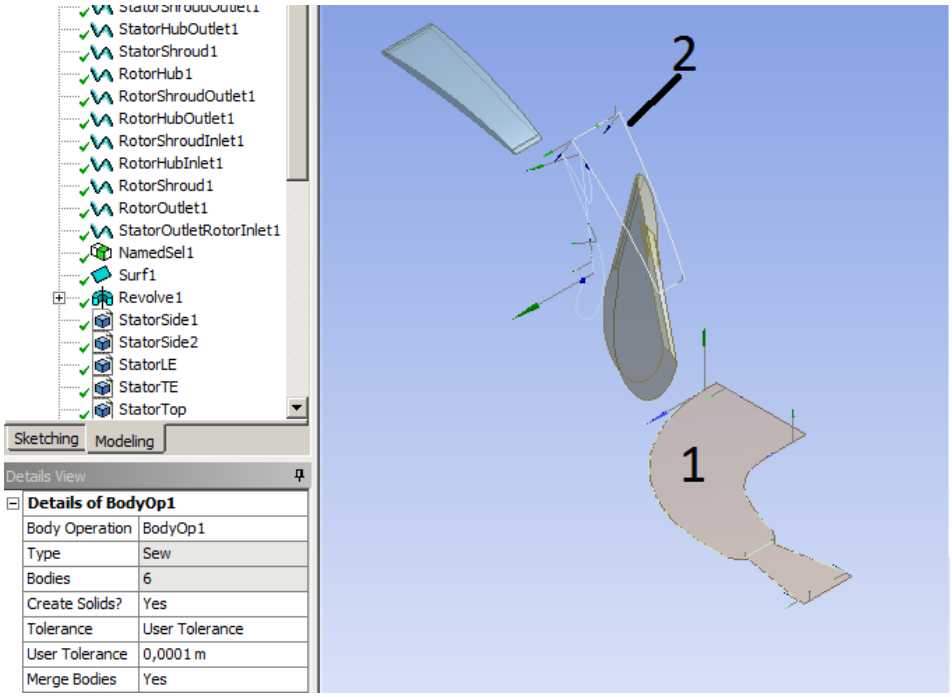

Figure A.1: Geometry after the script file has been run

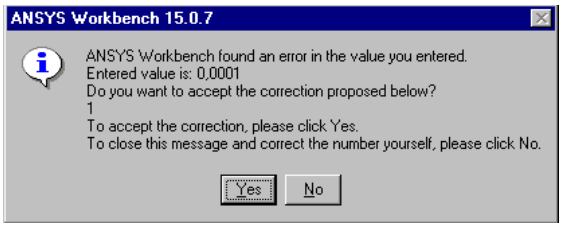

Figure A.2: Error message due to decimal separator

The next step is to create the FlowPath which is exported to TurboGrid™. It is recommended to suppress the lines and surfaces that are not used.

- Expand *6 Parts, 6 Bodies* in the tree outline seen in Figure A.3
- Control click (Hold ctr button and left mouse click) to highlight the 3 *Line Bodies* and the *Surface Body*
- Right click one of the bodies and select *Suppress Body*

Sketches for the *Flow Path* need to be created. Start by looking at the geometry in meridional view.

- Click the *y-axis* in the bottom right corner
- Open the sketching tab seen in Figure A.3

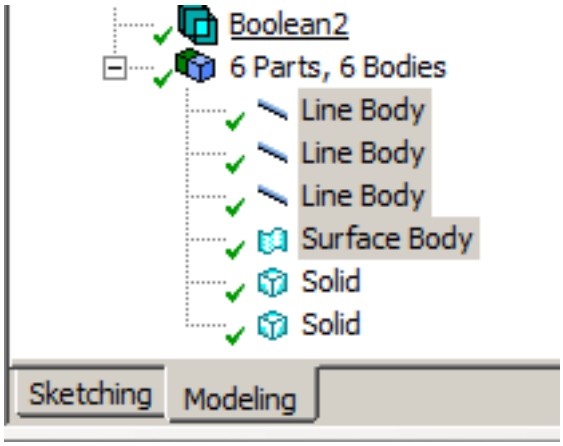

Figure A.3: Sketching tab and the bodies to suppress

- In *Constraints*, check both boxes (*Global* and *Cursor*) in *Auto Constraints* as in Figure A.4
- Open the *Modify* tab, and select *Duplicate* (Figure A.4
- Activate the appropriate sketch. Select *StatorHub* in the tab in the red circle in Figure A.4
- Left click the 3 lines in the stator hub (see Figure A.5)
- Right click and select duplicate selection as in Figure A.6
- Activate the next sketch. Select *StatorHub* in the tab in the red circle in Figure A.4
- Left click the 3 lines in the stator shroud (see Figure A.5)
- Right click and select duplicate selection
- Activate the next sketch. Select *StatorInlet* in the tab in the red circle in Figure A.4
- Left click the inlet of the stator (see Figure A.5)
- Right click and select duplicate selection

The stator outlet and rotor inlet share a boundary. This boundary has to be created.

- Activate the appropriate sketch. Select *StatorOutletRotorInlet* in the tab in the red circle in Figure A.4
- In the tab above *Modify*, open the *Draw* tab, see Figure A.7
- Select *Line*

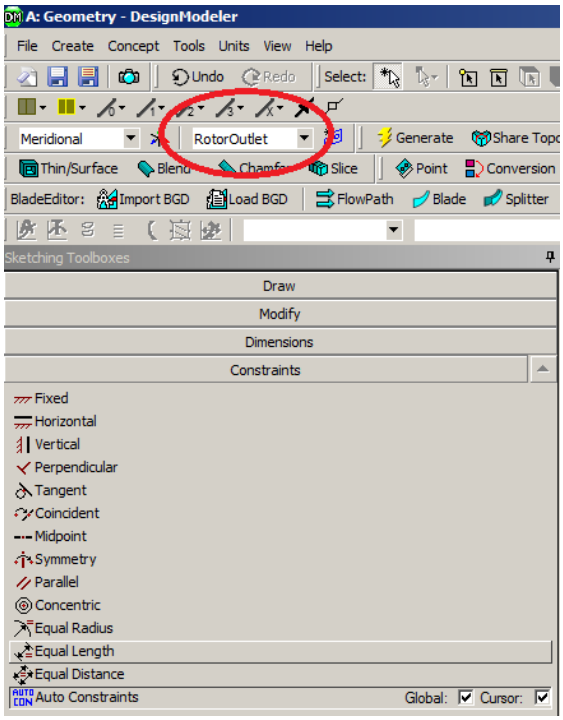

Figure A.4: Select the constraints and choose the correct sketch

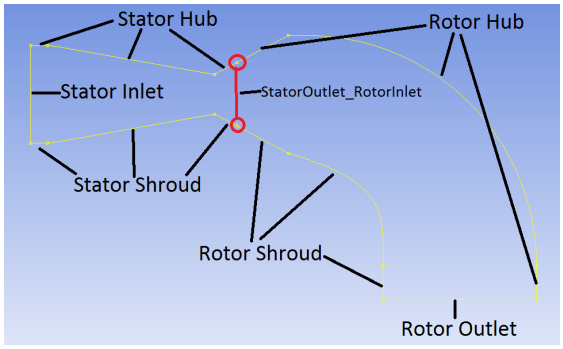

Figure A.5: Definition of inlet, hub, shroud and outlet of the flow paths

- By hoovering the mouse over the upper point (inside a red circle in Figure A.5) in the intersection, the letter *P* indicates that the line will be connected to the point as in Figure A.8
- Click the upper point
- Click the lower point to create the line
- The letter *H* should appear to the left of the line, indicating that the line is horizontal

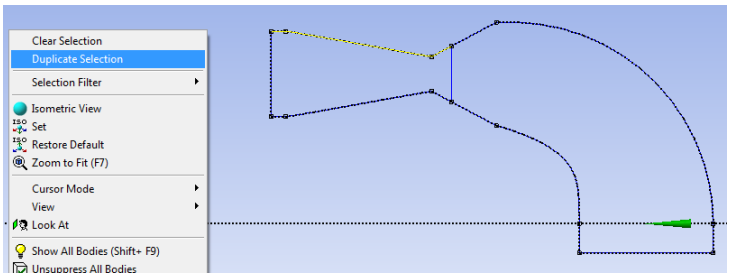

Figure A.6: Create the stator hub

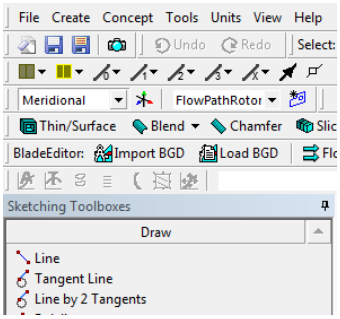

Figure A.7: Open the *Draw* tab

- If the letter *C* appears instead of the *P*, delete the line and draw it again

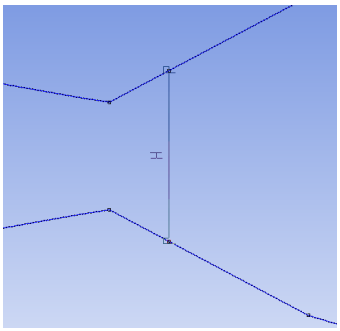

Figure A.8: Stator outlet and rotor inlet

The flow path for the stator should now be fully defined. Continue and define the rotor the same way as the stator. The rotor inlet is the same as the stator outlet. Go back to the *Modeling* tab (Figure A.3).

- Create a new *FlowPath* by clicking FlowPath, seen in Figure A.9
- Rename the feature to *FlowPathStator* as seen in A.10
- Click the text *Not selected* next to *Hub Contour*

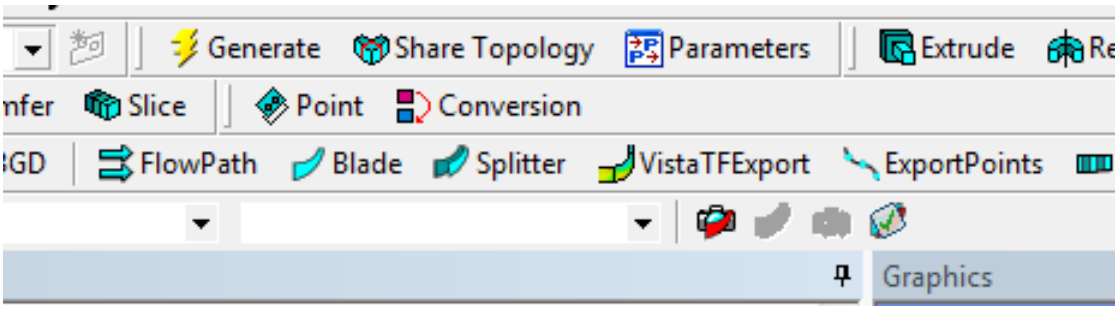

Figure A.9: *BladeEditor features*

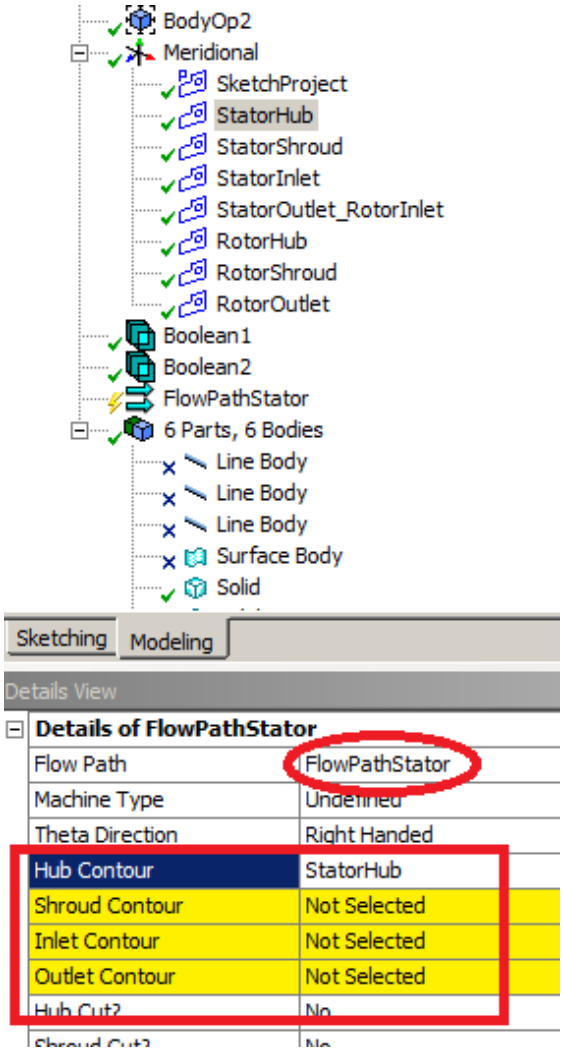

Figure A.10: Flow Path definition

- Click the *StatorHub* sketch under the *Meridional* tab in the tree outline, and click apply
- Click the text *Not selected* next to *Shroud Contour*
- Click the *StatorShroud* sketch under the *Meridional* tab in the tree outline, and click apply
- Click the text *Not selected* next to *Inlet Contour*
- Click the *StatorInlet* sketch under the *Meridional* tab in the tree outline, and click apply
- Click the text *Not selected* next to *Outlet Contour*
- Click the *StatorOutletRotorInlet* sketch under the *Meridional* tab in the tree outline, and click apply
- Press F5 on the keyboard to generate the feature

The same procedure is done for the rotor:

- Create a new *FlowPath* by clicking FlowPath, seen in Figure A.9
- Rename the feature to *FlowPathRotor*
- Click the text *Not selected* next to *Hub Contour*
- Click the *RotorHub* sketch under the *Meridional* tab in the tree outline, and click apply
- Click the text *Not selected* next to *Shroud Contour*
- Click the *RotorShroud* sketch under the *Meridional* tab in the tree outline, and click apply
- Click the text *Not selected* next to *Inlet Contour*
- Click the *StatorOutletRotorInlet* sketch under the *Meridional* tab in the tree outline, and click apply
- Click the text *Not selected* next to *Outlet Contour*
- Click the *RotorOutlet* sketch under the *Meridional* tab in the tree outline, and click apply
- Press F5 on the keyboard to generate the feature

When the flow paths have been created, the geometry is exported to TurboGrid™. This is done with the *ExportPoints* feature.

- Click *ExportPoints*, seen in Figure A.9
- Rename the feature to *ExportPointsStator*
- Click the empty field next to *Blade or Flow Path*
- Select *FlowPathStator* created previously
- Click apply
- Specify the Number of Blades
- The *Blade Row Number* for the stator is 1
- Click the empty field next to *Blade Surfaces*
- Hold the right mousebutton while clicking the left to get the box select tool
- Select the stator
- Hold the right mousebutton while clicking the left to get the surface selection tool again
- Deselect the hub and shroud by holding down the ctr key and left click the surface
- The model can be revolved by holding down the scroll button
- Click apply and generate (press F5)

The same procedure is done for the rotor:

- Click *ExportPoints*, seen in Figure A.9
- Rename the feature to *ExportPointsRotor*
- Click the empty field next to *Blade or Flow Path*
- Select *FlowPathRotor* created previously
- Click apply
- Specify the *Number of Blades*
- The *Blade Row Number* for the rotor is 2
- Click the empty field next to *Blade Surfaces*
- Hold the right mousebutton while clicking the left to get the box select tool
- Select the rotor

- Hold the right mousebutton while clicking the left to get the surface selection tool again
- Deselect the hub and shroud by holding down the ctr key and left click the surface
- The model can be revolved by holding down the scroll button
- Click apply and generate (press F5)

Close DesignModeler™. To edit the features in case an error occurs, right click the

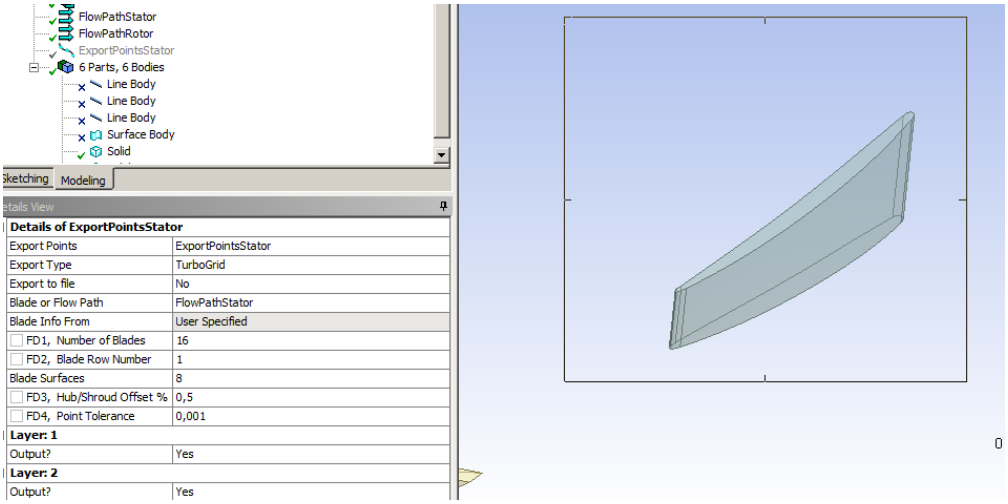

Figure A.11: Export the stator and rotor blades with ExportPoints

feature and select *Edit Selections* and do the appropriate changes.

A.2 TurboGrid™

The script for TurboGrid™, *WorkbenchTG_out.wbjn*, is run. The script creates two TurboGrid™ cells, one for the stator and one for the rotor. For this to work, it is important to define the correct names for the Flow Path in DesignModeler™. To run the script, select *File* > *Scripting* > *Run script file...* and open *TurboGrid_out*.

The mesh quality can be checked by expanding the *Mesh Analysis* tab in the tree outline in TurboGrid™, and double click *Mesh Statistics*. An approximation of the y^+ value can be seen by double clicking *Mesh data* and open the passage tab. If the value is to large, the *Factor Base* or *Factor ratio* parameters can be increased. When the mesh quality and y^+ has been checked TurboGrid™ is closed.

If for some reason the TurboGrid™ script fails, make sure that the input for the stator is defined as shown in Figure A.12 and the rotor in similar way, with Flowpath defined as FlowPathRotor and Bladerow Number 2.

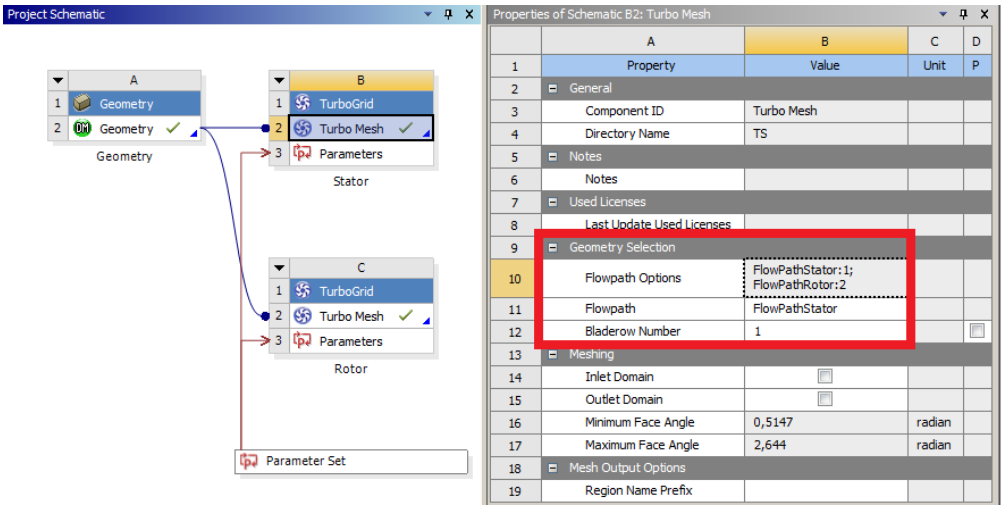

Figure A.12: Definition of the TurboGrid™ input. Blade row number 1 and FlowPath-Stator for the stator mesh, Blade row number 2 and FlowPathRotor for the rotor

A.3 CFX™

From Worbench™ the script file *WorkbenchCFX_out.wbjn* is run the same way as for the geometry and mesh to set up the boundary conditions and boundary definitions. The working fluid has to be selected manually in CFX. When the script is complete and the fluid has been selected the solution cell can be opened by right clicking and select edit. Check the box for double precision and start the run.

Appendix B

Appendix 2 - FT Guide

For geometry generation and meshing of all domains for the FT model the process of running each script is started in the same way. A script file is loaded to ICEM CFD™ and then run through it. Figure B.1a shows where to go when loading a script in ICEM CFD™ and Figure B.1b the replay control window is shown. To load the desired script file, one should press the *load* button, choose the right script and click *Do all*. ICEM CFD™ should run through every command in the script, creating the geometry or the mesh. The geometry and the mesh scripts have to be run separately. First the geometry is created and then the mesh is generated on top of the geometry

For every domain the most common procedures will be described to some extent but since the geometry can be varying it is hard to specify one procedure that works every time. What is common with all of the domains is the export of the mesh. Figure B.2 shows how to create an unstructured mesh. First right-click on the *Pre-Mesh* feature and select *Convert to Unstructured Mesh*.

Next is to export the mesh from ICEM CFD™ to a format CFX™ can read. By following Figure B.3 the mesh will be exported. The underlined parts should represent the project name and path. The former with a *.fbc* format and *.cfx5* format.

For all the domains a preliminary mesh element size and near wall treatments are specified according to the Reynolds number in the Matlab™ code *changeLines.m*. This is a global setting that might be needed to change after running the script for the volute to achieve highest quality of the mesh.

B.1 Volute

For the volute the text file *Volute1Out.rpl* is loaded and run like described above. When the script has finished the mesh script *VoluteAllSectionOgridOut.rpl* is loaded an run. Now the volute geometry and mesh should be done. It is a good procedure to follow up by checking all the angles and determinants for the mesh quality. The volute should look

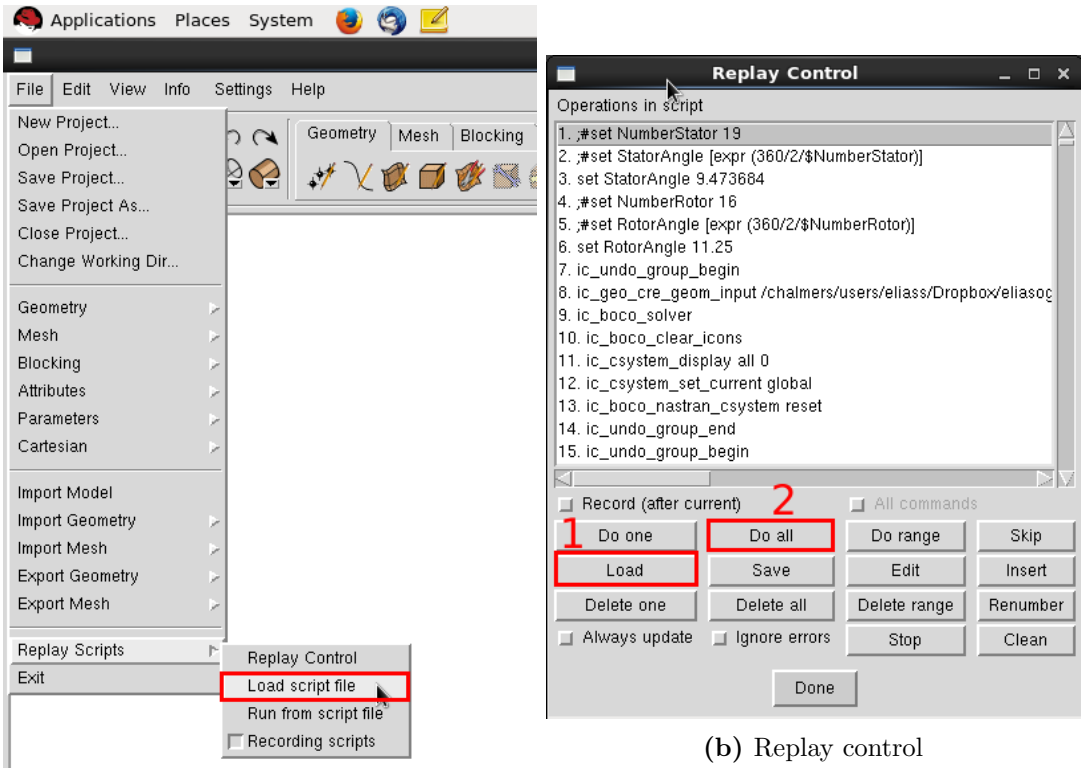

(a) Load script

(b) Replay control

Figure B.1: First steps in ICEM CFD™

close to Figure B.4 where the procedure of checking the angle is shown. Some angles are below 20° but since those elements are few and above 10° the mesh should be acceptable but could be improved. The more time spent on each mesh improves the mesh quality.

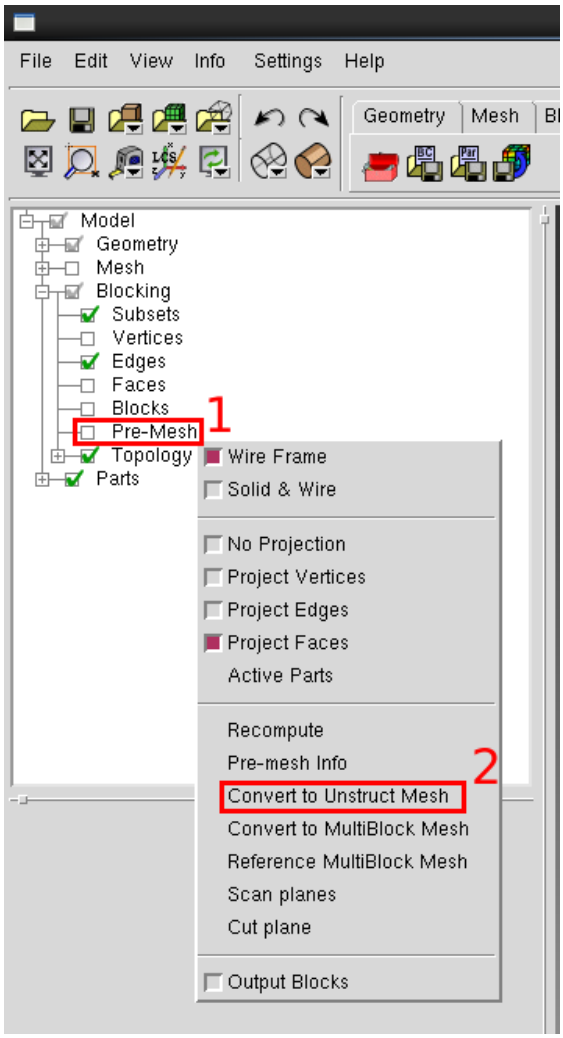

Figure B.2: Unstructured mesh

B.2 Stator

For the stator the text file *STATOROut.rpl* is loaded an run like described before. When the script has finished with the geometry the mesh script *STATORMESHOut.rpl* is loaded and run. After this the stator mesh should be close to done. There might be a need for moving some control points to gain acceptable quality of the mesh.

B.2.1 Stator mesh

There are some procedures that can make it easier to generate high quaility mesh.

Since the stator domain is the same at hub and shroud the mesh should be thought

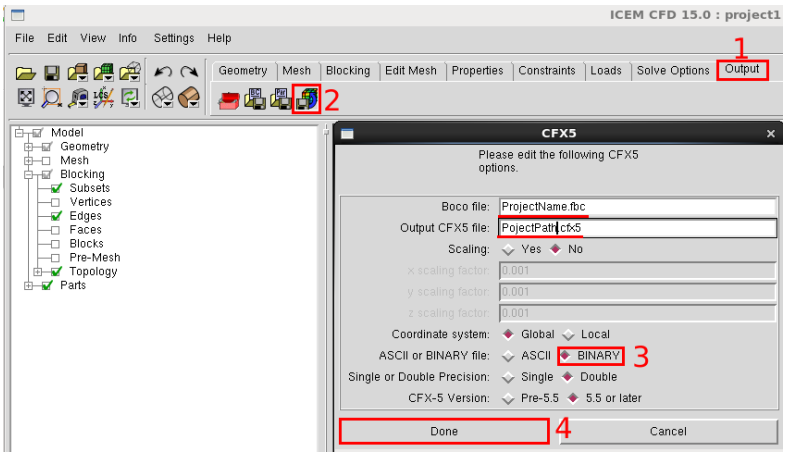

Figure B.3: CFX5 file format

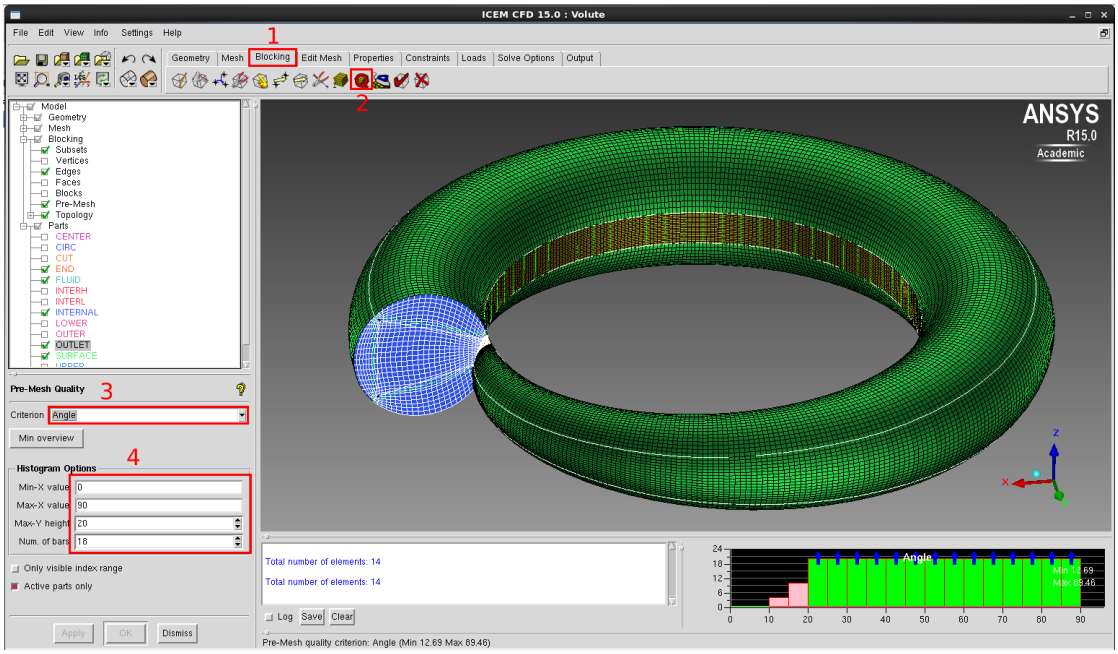

Figure B.4: Volute

of as 2D, i.e. the mesh of the hub and shroud surfaces should be the same. Figure B.5 shows how this can be accomplished. It can be used at any time of the editing of the mesh. This operation makes the unselected vertex at the end of the line, in 5, to go directly below the selected vertex, 7, by changing the XY coordinates of the vertex.

To move the O-grid vertices the pre-mesh at hub and shroud should be turned on since the O-grid vertices are connected to the surfaces. After doing this, it is good to keep the

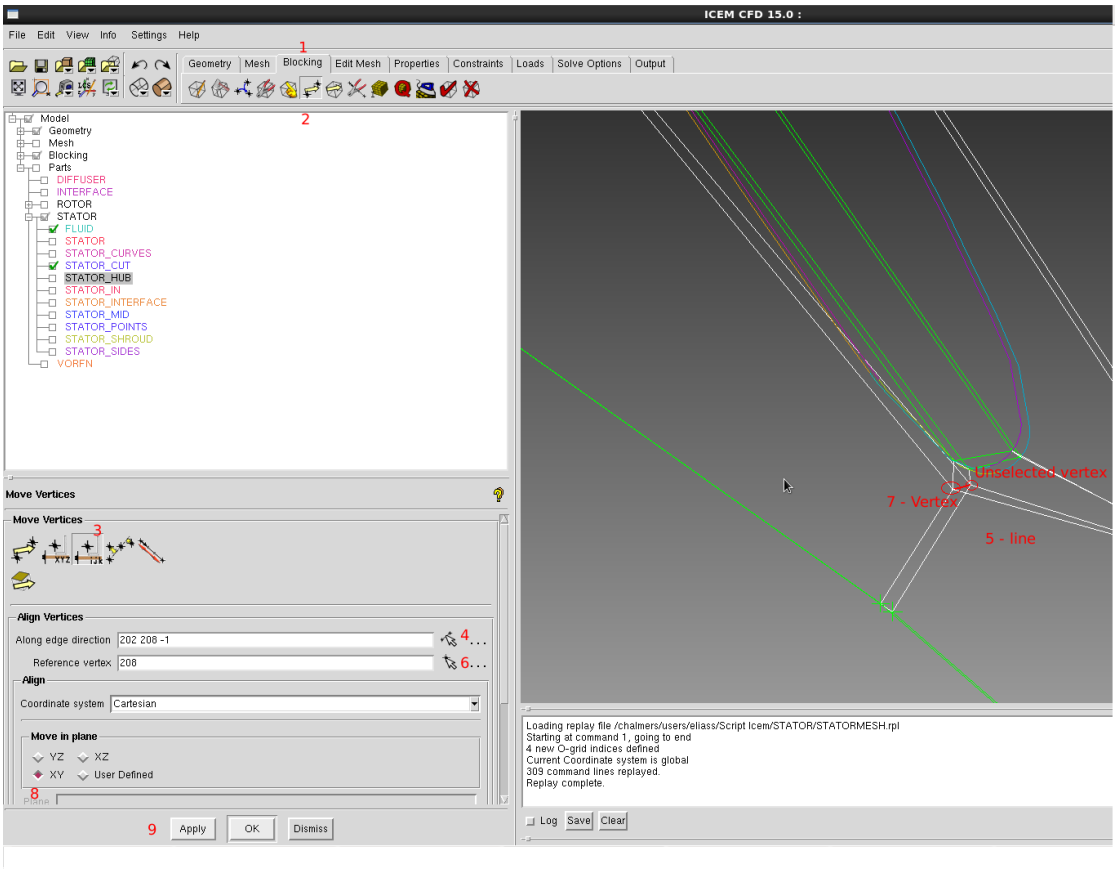

Figure B.5: Align

view in the XY plane and to only use the *Multiple* option at point 3 in Figure B.6. In the figure the five vertices that can be modified on the blade are highlighted with a circle.

When a high quality mesh has been generated for the stator domain, the mesh should be converted to unstructured mesh and exported to a *.cfx5* format liked described before.

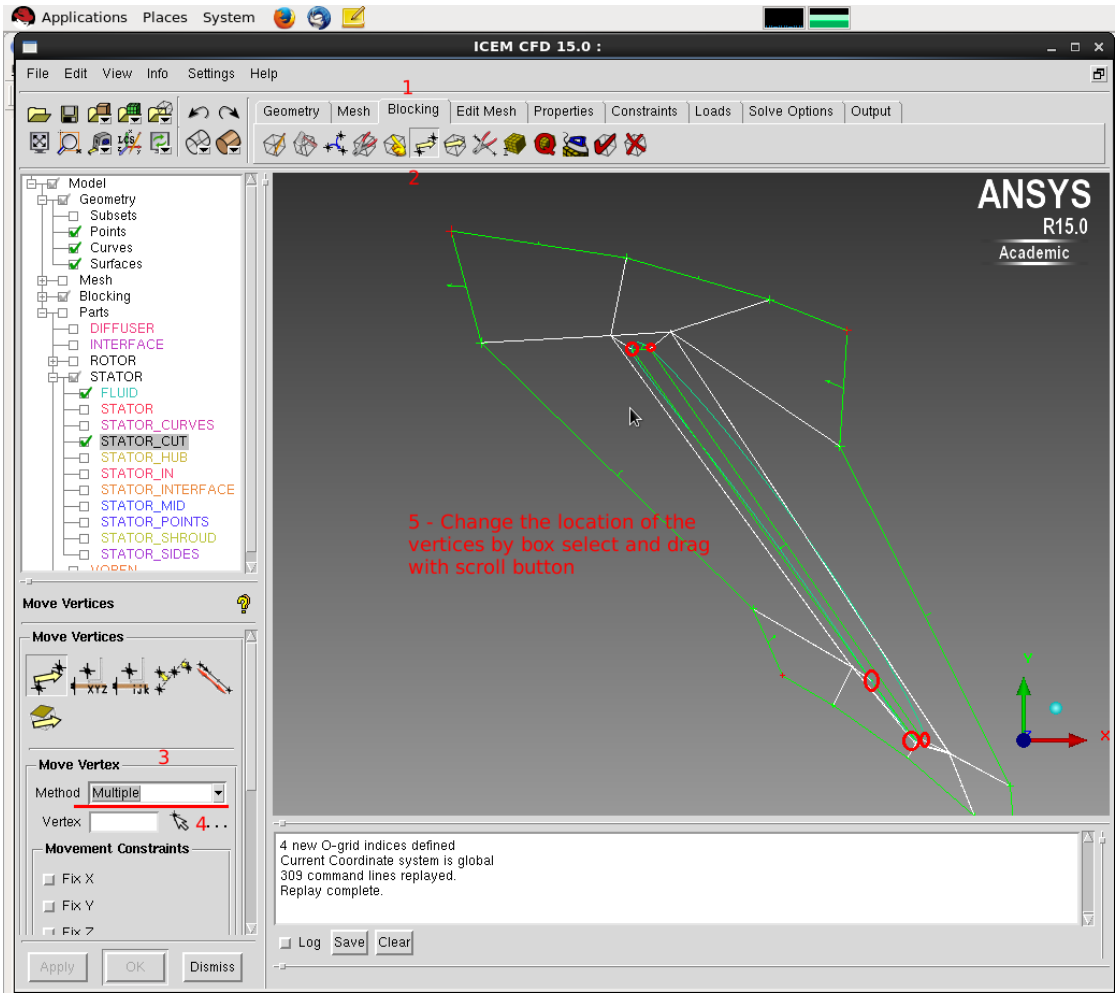

Figure B.6: Z-Plane

B.3 Rotor

Before running the script to generate the rotor geometry and mesh, a parameter can be changed that specifies if there should be a shift of the inlet at hub and shroud. In Figure B.7 the rotor inlet for the NASA case is shown with no shift. This causes the right and left sides to have equally distance from the blade at both hub and shroud. In Figure B.8 the rotor inlet for the ORC case is shown with 4° shift. This causes the left side at the hub to be closer to the blade than the right side but the right side at the shroud is closer than the left side. This is done to minimize the risk of to skewed angles at the inlet surface. Since this will decrease the area on the left side of the hub, there is a limit on how much one can shift the inlet.

For the rotor the text file *ROTOROut.rpl* is loaded an run like described before. When

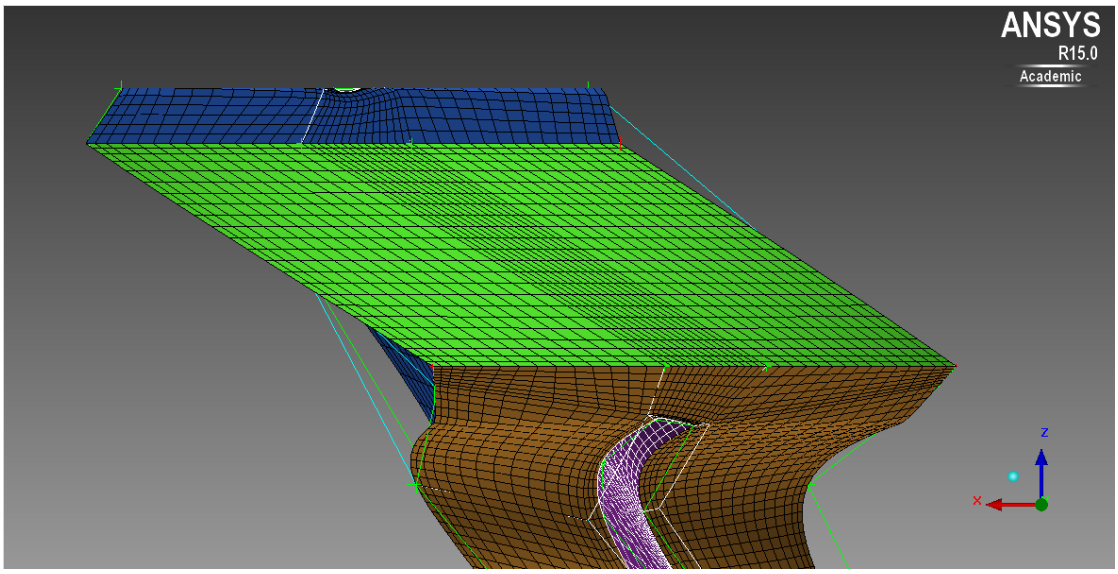

Figure B.7: Rotor inlet of the NASA case

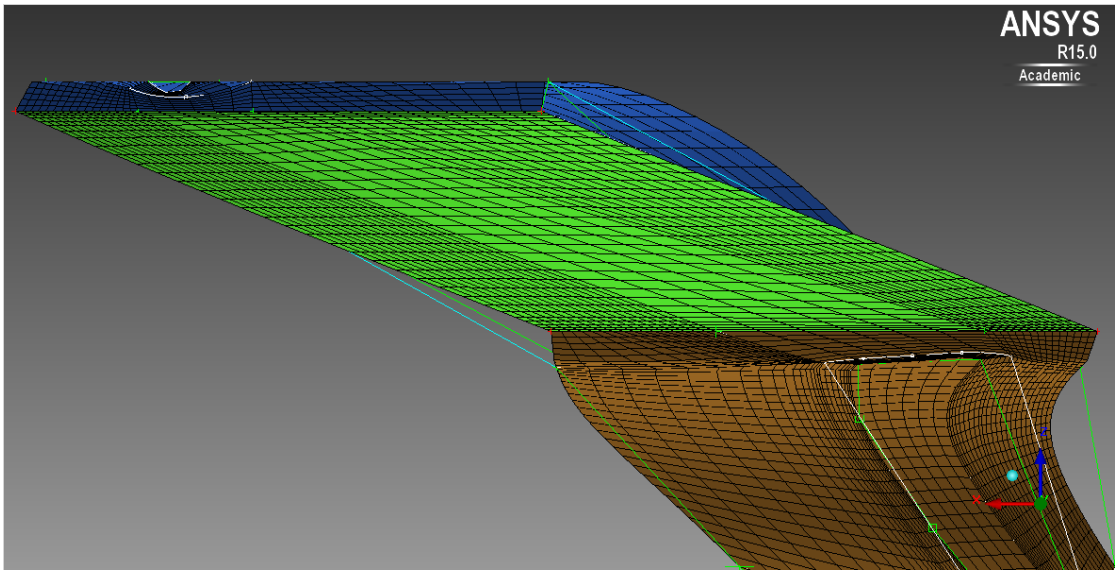

Figure B.8: Rotor inlet of the ORC case

the script has finished with the geometry the mesh script *ROTORMESHOut.rpl* is loaded and run. After this the rotor mesh should be close to done. There might be a need for moving some control points to gain acceptable quality of the mesh.

B.3.1 Rotor Mesh

Meshing the rotor is more complicated since it is more three dimensional than the other domains. Therefore it is recommended to create the other domains first, before meshing the rotor domain, for practicing. When specifying the number of nodes on each edge use Geometry1 instead of BiGeometry and copy to all parameters.

B.4 Diffuser

Before running the script to generate the diffuser geometry and mesh, two parameters can be set to make the meshing more automatic. In Figure B.9 the locations of those planes are shown. The diffuser inlet, higher control surface and the lower control surface are shown. In the Matlab™ code *UpdateFullTurbine.m* the height of those surfaces are specified as a function of the height difference between the cone tip and the diffuser inlet, the red line. The variables are called *HigherVariable* and *LowerVariable* and can be modified as needed. One additional parameter is to specify where on the cone the diffuser inlet is, i.e. at what height. For the diffuser the text file *DiffuserOut.rpl* is loaded

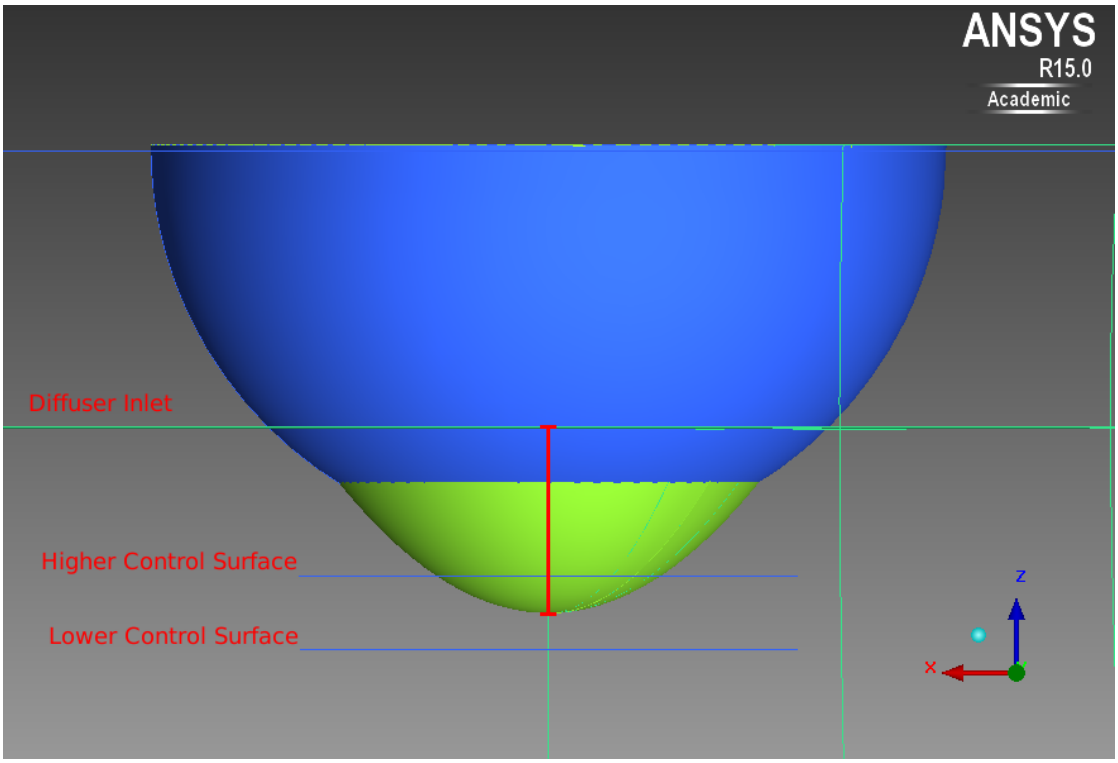

Figure B.9: Diffuser control planes

and run like described before. When the script has finished with the geometry the mesh script *DiffuserOut.rpl* is loaded and run. After this the diffuser mesh should be close to done. There might be a need for moving some control points to gain acceptable quality of the mesh. If the control surfaces are well located the mesh should need minimum amount of adjustments for high mesh quality.

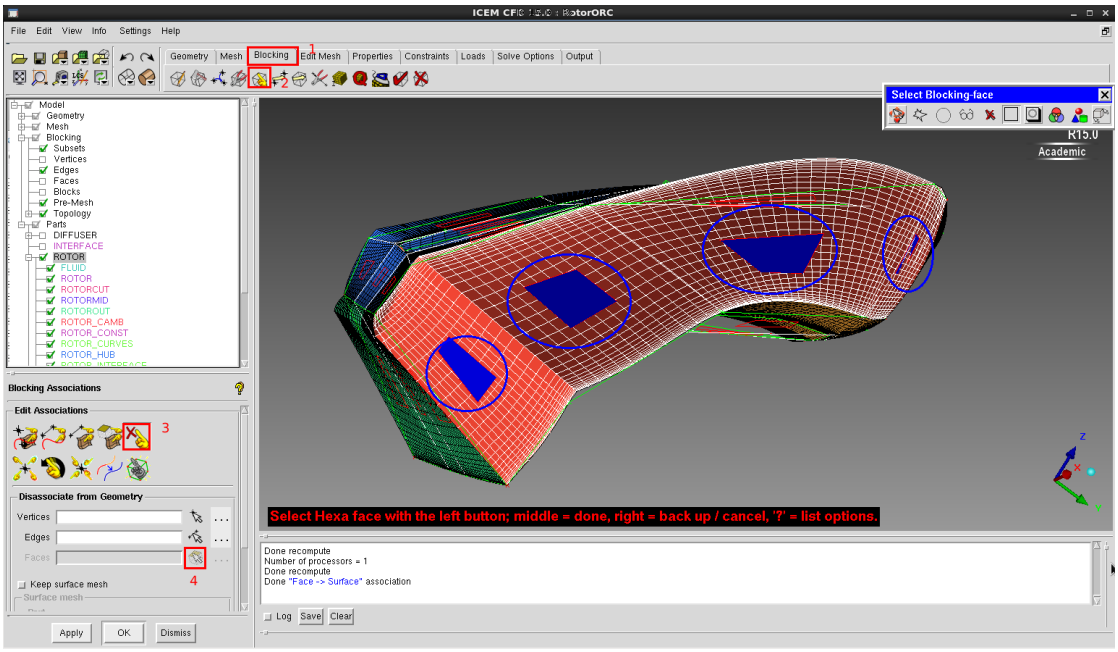

Figure B.10: Remove the associations between the mesh domain sides and the geometry

B.5 360° Stator and Rotor

Making the 360° stator and rotor domains require a few extra steps.

1 Removing the surface association from the geometry for the 360° domain to have no internal interfaces. Figure B.10 shows how to remove the associations from the sides. One has to deselect the four surfaces marked in the figure with blue circles on both sides.

2 Rotate the domain to fill up the 360° domain. Figure B.11 shows the process of rotating the mesh. First all the domain is selected, this is done by selecting the box marked with 3, moving the mouse over the model and press the a button. The copy box is then checked and the number of copies specified and the number should be one less than the total number of domains.

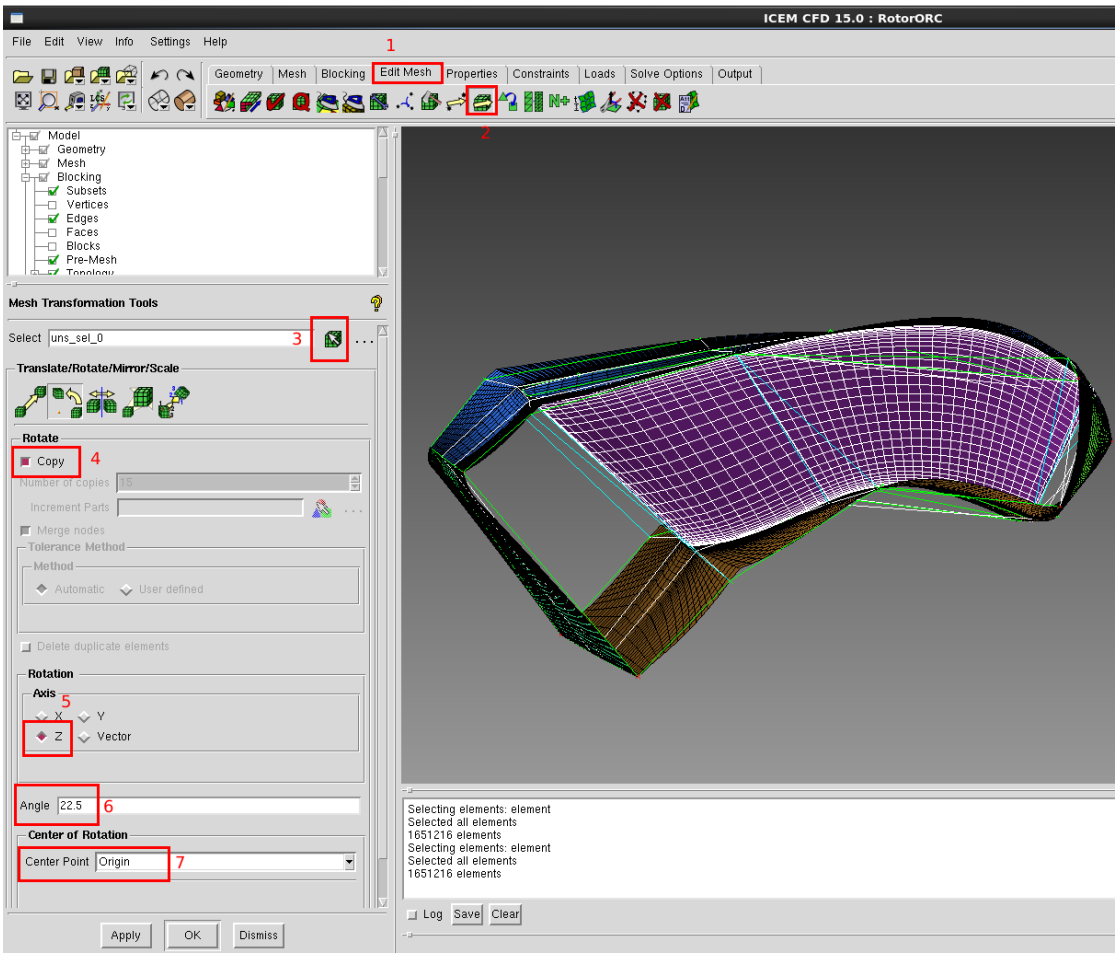

Figure B.11: Rotating the mesh